ENERGY STABLE MODEL REDUCTION OF NEURONS BY NONNEGATIVE DISCRETE EMPIRICAL INTERPOLATION[*]

DAVID AMSALLEM[†] AND JAN NORDSTRÖM[‡]

Abstract. The accurate and fast prediction of potential propagation in neuronal networks is of prime importance in neurosciences. This work develops a novel structure-preserving model reduction technique to address this problem based on Galerkin projection and nonnegative operator approximation. It is first shown that the corresponding reduced-order model is guaranteed to be energy stable, thanks to both the structure-preserving approach that constructs a distinct reduced-order basis for each cable in the network and the preservation of nonnegativity. Furthermore, a posteriori error estimates are provided, showing that the model reduction error can be bounded and controlled. Finally, the application to the model reduction of a large-scale neuronal network underlines the capability of the proposed approach to accurately predict the potential propagation in such networks while leading to important speedups.

Key words. model reduction, nonnegative reduced basis, discrete empirical interpolation, Hodgkin–Huxley equation, summation-by-parts operators

AMS subject classification. 37M99

DOI. 10.1137/15M1013870

1. Introduction. Being capable of performing fast and accurate predictions of the potential propagation in neurons is of prime importance in neurosciences. Recent approaches include the development of electronic circuits that mimic the neuronal networks [BGM+14] as well as the numerical solution of nonlinear partial differential equations (PDEs) associated with the potential propagation [HH52, Hin84, KCSC10, AR11, AN13]. The differential equations associated with the propagation of potential in neurons were developed in the seminal work of Hodgkin and Huxley [HH52]. The numerical solution of the resulting coupled system of ordinary differential equations (ODEs) and PDEs become, however, quickly intractable when the dimension of the associated discretized system become large. Model reduction techniques [KCSC10, AR11] can alleviate that computational burden by limiting the solution space to a subspace of small dimension.

An important aspect associated with the simulation of the propagation of potential in a neuronal network by a finite differences scheme such as in [Hin84, AN13] is the stability of the scheme. In [AN13], the authors develop energy stable high-order finite difference schemes based on summation-by-parts operators that approximate the Hodgkin–Huxley equations.

Efficient model reduction approaches for reducing the cost associated with solving the Hodgkin–Huxley equations are developed in [KCSC10] and [AR11]. However, no stability results associated with the proposed approaches were presented. Furthermore, the underlying finite difference scheme was restricted to be of second order. The goal of the present paper is to develop a model reduction approach based on

high-order finite difference schemes that preserves the energy stability properties established in [AN13] while leading to significant computational speedups.

Preservation of stability in model reduction is an important topic that has been studied in the case of equations arising in electrical engineering [BD09], incompressible flows [RV07], the advection-diffusion equation [UP14, DPW14], linearized computational fluid dynamics (CFD) [BKST09], linearized aeroelasticity [AF13], and nonlinear CFD in [AFZ13]. Stabilization techniques have also been developed for generic linear systems in [AF12]. In the present paper, stability of the reduced-order model (ROM) is established in the sense of energy stability, similarly as in [BKST09] for linearized CFD.

In this paper, the equations of interest are nonlinear and energy stability is enforced by a novel method based on the combination of Galerkin projection and the accurate approximation of positive nonlinear terms by nonnegative bases. The approach combines this nonnegative basis together with the discrete empirical interpolation method. A drawback of an approximation by positive functions is that it is usually associated with a slow convergence. However, the present work establishes that, by using these positive functions energy stability of the underlying finite difference scheme carries over to the ROM scheme. Furthermore, a posteriori error bounds are developed, providing an estimation of the error associated with the reduced scheme.

This paper is organized as follows. The PDEs associated with the propagation of potential in neurons are presented in section 2 together with associated boundary conditions (BCs). The semidiscrete scheme, initially established in [AN13] is briefly reviewed in section 3. Galerkin projection-based model reduction of the semidiscrete scheme is developed in section 4 together with a stability result. The construction of the reduced basis associated with the ROM is addressed in section 5. The efficient model reduction of the nonlinear term, requiring a special treatment by nonnegative basis approximation is developed in section 6. A posteriori error estimates are provided in section 7. Finally the application of the model reduction approach to a neuronal network with more than 15,000 degrees of freedom is presented in section 8 and conclusions are given in section 9.

2. The continuous problem.

2.1. Networks in neurons. A network of connected dendrites, soma, and axons is considered in this paper. The goal is to determine the potential distribution and propagation in the neuron components. For that purpose, the Hodgkin–Huxley equations based on the cable equation [HH52] are solved. These are a set of coupled PDEs and ODEs expressed in terms of (1) the intracellular potential u and (2) three gating variables m, h, and n that describe the dynamics associated with the ion channels. More specifically, m and h, respectively, specify the activation and inactivation of the sodium channels and n specifies the activation of the potassium channels.

2.2. Equations for a single cable. In this section only, a single cable in the computational domain $[0, \mathcal{L}]$ is considered. The equation governing the distribution of potential u is [KS09]

$$(2.1) \qquad u_t = \frac{\mu}{a(x)} \left(a(x)^2 u_x \right)_x - \frac{1}{C_m} g(m, h, n)u + \frac{1}{C_m} f(m, h, n, x, t),$$

where $(x, t) \in [0, \mathcal{L}] \times [0,\ T]$. The radius of the neuron at location x is $a(x)$, C_m is

the specific membrane capacitance, and μ the ratio

$$(2.2) \qquad \mu = \frac{1}{2C_m R_i} > 0$$

with R_i denoting the axial resistivity. The conductance

$$g(x,t) = g(m(x,t), h(x,t), n(x,t))$$

of the cable is expressed as a polynomial function of the three gating variables m, h, and n:

$$(2.3) \qquad g(m,h,n) = g_1 m^3 h + g_2 n^4 + g_3 > 0,$$

where the coefficients g_ℓ $\ell = 1, 2, 3$ are also strictly positive. The expression for the source term $f(m, h, n, x, t)$ is given by

$$(2.4) \qquad f(m, h, n, x, t) = g_1 E_1 m^3 h + g_2 E_2 n^4 + g_3 E_3 - i(x,t),$$

where E_ℓ, $\ell = 1, 2, 3$, are equilibrium potentials and $i(x,t)$ is an input current at location x. In this paper, the input current is assumed to be localized and limited to a small number N_s of sources centered at locations $x = x_s$, $s = 1, \ldots, N_s$, corresponding, for instance, to synaptic input. Hence,

$$(2.5) \qquad i(x,t) = \sum_{s=1}^{N_s} i_s(x,t), \ x \in [0, \mathcal{L}].$$

Each source is in practice localized to a small neighborhood of its center location x_s. Equation (2.1) is coupled with a set of three ODEs describing the evolution of the gating variables:

$$(2.6) \qquad \begin{cases} m_t = \alpha_m(u(x,t))(1 - m(x,t)) - \beta_m(u(x,t))m(x,t), \\ h_t = \alpha_h(u(x,t))(1 - h(x,t)) - \beta_h(u(x,t))h(x,t), \\ n_t = \alpha_n(u(x,t))(1 - n(x,t)) - \beta_n(u(x,t))n(x,t), \end{cases}$$

where $(x,t) \in [0, \mathcal{L}] \times [0, T]$. Expressions for α_m, α_h, α_n, β_m, β_h, and β_n were determined for the giant squid axon in [HH52], and are reported in Appendix A.

Several types of BCs can be associated with the cable equation [KS09]. They are described in the following section.

2.3. BCs. Three different types of BCs for (2.1) are considered in this paper. The first one is enforced when the cable is connected to the soma, the second one when there is a junction between multiple cables, and the third one when the extremity of the cable is not connected.

2.3.1. Soma. Because of the relatively large size of the soma, the potential and gating variables are assumed to be uniform in it. As a result, the presence of the soma will be modeled as a BC applied to the cables connected to it.

The soma BC describes the current conservation in the soma located at an extremity $x_s \in \{0, \mathcal{L}\}$ [KS09]:

$$(2.7) \qquad (u)_t = -\eta a^2 \nabla u \cdot \mathbf{n}_s - \frac{1}{C_m} g(m, n, h) u + \frac{1}{C_m} f(m, n, h, x, t), \ x = x_s$$

with

$$(2.8) \qquad \eta = \frac{\pi}{A_{\text{soma}} R_i C_m} > 0$$

and A_{soma} denotes the soma surface area. $\mathbf{n}_s$ denotes the outer normal vector to $[0, \mathcal{L}]$
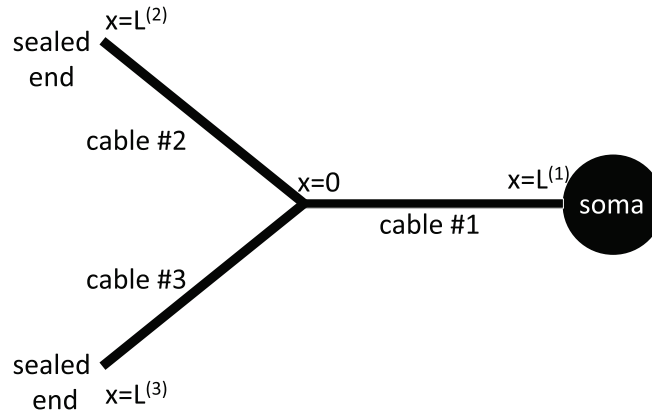
FIG. 1. *Model network.*

at the end point $x = x_s$ of the cable. Note the similarity between the BC (2.7) and the PDE (2.1).

2.3.2. Junction. Interface conditions are applied when multiple cables meet at a common junction. These conditions enforce potential continuity and current conservation [KCSC10]. If N_c cables of respective potentials $u^{(c)}$, $c = 1, \ldots, N_c$, and cable radii $a^{(c)}(\cdot)$ join at $x = x_b$, the interface conditions for potential continuity are

$$(2.9) \qquad u^{(c_1)}(x_b, t) = u^{(c_2)}(x_b, t) \ \forall c_1, c_2 \in \{1, \ldots, N_c\}, \ c_1 \neq c_2,$$

and for current conservation

$$(2.10) \qquad \sum_{c=1}^{N_c} (a^{(c)}(x_b))^2 \nabla u^{(c)}(x_b, t) \cdot \mathbf{n}^{(c)}(x_b) = 0.$$

Consequently, there is a total of $\frac{N_c(N_c-1)}{2} + 1$ interface conditions at a single junction.

2.3.3. Sealed end. The sealed end BC states that there is no current exiting the neuron at $x_b = 0$ or $\mathcal{L}$. It is

$$(2.11) \qquad \nabla u(x_b, t) \cdot \mathbf{n}(x_b) = 0.$$

2.4. Model network. Without loss of generality, a model network of three cables connected to a soma is considered in the following sections. Different and significantly larger networks will be considered in the numerical applications in section 8 and the analysis of the three cable connections generalizes directly to the larger networks. The model network is depicted in Figure 1. For a network of N_c neuron cables—dendrites and/or axons—a superscript $^{(c)}$, $c = 1, \ldots, N_c$, will denote the quantities of interest relevant to the cth cable.

2.4.1. Equations. The equations governing the potential propagation in the network are all of the type (2.1) and (2.6). The cables are connected to each other at $x = 0$ and the other extremities are either sealed or connected to the soma:

$$(2.12) \qquad \begin{aligned} u_t^{(c)} &= \frac{\mu}{a^{(c)}\left(x^{(c)}\right)} \left(\left(a^{(c)}\left(x^{(c)}\right) \right)^2 u_x^{(c)} \right)_x - \frac{1}{C_m} g\left(m^{(c)}, h^{(c)}, n^{(c)}\right) u^{(c)} \\ &\quad + \frac{1}{C_m} f\left(m^{(c)}, h^{(c)}, n^{(c)}, x^{(c)}, t\right), \end{aligned}$$

$$(2.13) \quad \begin{cases} m_t^{(c)} = \alpha_m \left(u^{(c)} \right) \left(1 - m^{(c)} \right) - \beta_m \left(u^{(c)} \right) m^{(c)}, \\ h_t^{(c)} = \alpha_h \left(u^{(c)} \right) \left(1 - h^{(c)} \right) - \beta_h \left(u^{(c)} \right) h^{(c)}, \\ n_t^{(c)} = \alpha_n \left(u^{(c)} \right) \left(1 - n^{(c)} \right) - \beta_n \left(u^{(c)} \right) n^{(c)}, \ c = 1, \ldots, 3, \end{cases}$$

for $x^{(c)} \in \Omega^{(c)} = \left[0, \mathcal{L}^{(c)} \right]$ together with the BCs:

$$(2.14) \quad u_t^{(1)} \left(\mathcal{L}^{(1)} \right) = -\eta \left(a^{(1)} \left(\mathcal{L}^{(1)} \right) \right)^2 u_x^{(1)} \left(\mathcal{L}^{(1)} \right)$$
$$- \frac{1}{C_m} g \left(m^{(1)} \left(\mathcal{L}^{(1)} \right), n^{(1)} \left(\mathcal{L}^{(1)} \right), h^{(1)} \left(\mathcal{L}^{(1)} \right) \right) u^{(1)} \left(\mathcal{L}^{(1)} \right)$$
$$+ \frac{1}{C_m} f \left(m^{(1)} \left(\mathcal{L}^{(1)} \right), n^{(1)} \left(\mathcal{L}^{(1)} \right), h^{(1)} \left(\mathcal{L}^{(1)} \right) \right) \quad \text{(soma BC)},$$

$$(2.15) \quad u_x^{(c)} \left(\mathcal{L}^{(c)} \right) = 0, \ c = 2, 3 \quad \text{(sealed BC)},$$

$$(2.16) \quad u^{(c_1)} (0) = u^{(c_2)} (0) \ \forall c_1, c_2 \in \{1, 2, 3\} \quad \text{(junction continuity BC)},$$

$$(2.17) \quad 0 = \sum_{c=1}^{3} \left(a^{(c)} (0) \right)^2 u_x^{(c)} (0) \quad \text{(junction conservation BC)}.$$

Well-posedness of the PDE associated with the model network has been established in [AN13].

PROPOSITION 1. *The initial boundary value problem* (2.12) *without source terms and with BCs* (2.14), (2.15), (2.16)*, and* (2.17) *is well-posed.*

3. The semidiscrete problem.

3.1. Semidiscretization in space. Considering again the case of the model network with 3 cables, (2.12) is discretized in each domain $\Omega^{(c)}$ using a uniform mesh of $N^{(c)} + 1$ points. The discrete approximation of the solution $u^{(c)}(\cdot, t)$ in $\Omega^{(c)}$ is then

$$(3.1) \quad \mathbf{u}^{(c)}(t) = \left[u_0^{(c)}(t), \ldots, u_{N^{(c)}}^{(c)}(t) \right]^T, \ u_j^{(c)}(t) \approx u^{(c)} \left(x_j^{(c)}, t \right),$$

where $x_j^{(c)} = \frac{j}{N^{(c)}} \mathcal{L}^{(c)}, \ j = 0, \ldots, N^{(c)}$. The semidiscrete version of (2.12) without inclusion of the BCs is, following [AN13],

$$(3.2) \quad \mathbf{A}^{(c)} \mathbf{u}_t^{(c)} = \mu \mathbf{D}_1^{(c)} \left(\left(\mathbf{A}^{(c)} \right)^2 \mathbf{D}_1^{(c)} \mathbf{u}^{(c)} \right) - \frac{1}{C_m} \mathbf{A}^{(c)} \mathbf{G}^{(c)}(t) \mathbf{u}^{(c)} + \frac{1}{C_m} \mathbf{A}^{(c)} \mathbf{f}^{(c)}(t),$$

where the diagonal matrix $\mathbf{A}^{(c)} = \mathbf{diag}(a_0^{(c)}, \ldots, a_{N^{(1)}}^{(c)})$ with $a_j^{(c)} = a(x_j^{(c)})$, the diagonal matrix $\mathbf{G}^{(c)}(t) = \mathbf{diag}(g_0(t), \ldots, g_{N^{(c)}}(t))$ with $g_j(t) = g(x_j^{(c)}, t)$, and $\mathbf{f}^{(c)}(t) = [f_0(t), \ldots, f_{N^{(c)}}(t)]$ with $f_j(t) = f(x_j^{(c)}, t)$.

The diagonal matrix $\mathbf{G}^{(c)}(t)$ approximating (2.3) is expressed as

$$(3.3) \quad \mathbf{G}^{(c)}(t) = g_1 \mathbf{diag} \left(\left(\mathbf{m}^{(c)}(t) \right)^3 \odot \mathbf{h}^{(c)}(t) \right) + g_2 \mathbf{diag} \left(\left(\mathbf{n}^{(c)}(t) \right)^4 \right) + g_3 \mathbf{I},$$

where $\mathbf{I}$ is the identity matrix and

$$(3.4) \quad \mathbf{m}^{(c)}(t) = \left[m_0^{(c)}(t), \ldots, m_{N^{(c)}}^{(c)}(t) \right]^T, \ m_j^{(c)}(t) \approx m^{(c)} \left(x_j^{(c)}, t \right).$$

The other vectors $\mathbf{h}^{(c)}(t)$ and $\mathbf{n}^{(c)}(t)$ are defined similarly. $\odot$ denotes the Hadamard product[1] and the power of a vector is considered entry by entry as $\mathbf{m}^3 = \mathbf{m} \odot \mathbf{m} \odot \mathbf{m}$. The forcing vector is

$$(3.5) \qquad \mathbf{f}^{(c)}(t) = g_1 E_1 \left(\mathbf{m}^{(c)}(t)\right)^3 \odot \mathbf{h}^{(c)}(t) + g_2 E_2 \left(\mathbf{n}^{(c)}(t)\right)^4 + g_3 E_3 \mathbf{1} - \mathbf{i}^{(c)}(t),$$

where $\mathbf{1}$ denotes a vector of ones. The current source approximating (2.5) is

$$(3.6) \qquad \mathbf{i}^{(c)}(t) = \sum_{s=1}^{N_s} i_s^{(c)}(t) \mathbf{i}_s^{(c)}.$$

$\mathbf{i}_s^{(c)}$ and $i_s^{(c)}(t)$ are the respective spatial and temporal distributions of the current originating from the sth source, as defined in (2.5).

The semidiscrete system can be written as a block system of equations as

$$(3.7) \qquad \mathbf{A}\mathbf{u}_t = \mu \mathbf{D}_1 \mathbf{A}^2 \mathbf{D}_1 \mathbf{u} - \frac{1}{C_m} \mathbf{A}\mathbf{G}(t)\mathbf{u} + \frac{1}{C_m} \mathbf{A}\mathbf{f}(t),$$

where each matrix has diagonal blocks, such as $\mathbf{A} = \mathbf{diag}(\mathbf{A}^{(1)}, \mathbf{A}^{(2)}, \mathbf{A}^{(3)})$, and each vector is of the form $\mathbf{u} = [\mathbf{u}^{(1)}, \mathbf{u}^{(2)}, \mathbf{u}^{(3)}]^T$.

Operators on a summation-by-parts form [KS74, KS75, Str94, CGA94, GKO95, NL13, NFA03, Mat12, Ols95a, Ols95b] approximate the derivative of $u^{(c)}(\cdot)$ as

$$(3.8) \qquad \mathbf{D}_1^{(c)} \mathbf{u}^{(c)} = \left(\mathbf{P}^{(c)}\right)^{-1} \mathbf{Q}^{(c)} \mathbf{u}^{(c)} = \left[u_{x0}^{(c)}, \ldots, u_{xN^{(c)}}^{(c)}\right]^T,$$

where $\mathbf{P}^{(c)}$ is a diagonal symmetric positive definite matrix and $\mathbf{Q}^{(c)}$ satisfies $\mathbf{Q}^{(c)} + (\mathbf{Q}^{(c)})^T = \mathbf{B}^{(c)} = \mathbf{diag}(-1, 0, \ldots, 0, 1)$.

In block form, defining global quantities on the entire network, we have

$$\mathbf{D}_1 = \begin{bmatrix} \mathbf{D}_1^{(1)} & \mathbf{0} & \mathbf{0} \\ \mathbf{0} & \mathbf{D}_1^{(2)} & \mathbf{0} \\ \mathbf{0} & \mathbf{0} & \mathbf{D}_1^{(3)} \end{bmatrix}, \ \mathbf{D}_2 = \begin{bmatrix} \mathbf{D}_2^{(1)} & \mathbf{0} & \mathbf{0} \\ \mathbf{0} & \mathbf{D}_1^{(2)} & \mathbf{0} \\ \mathbf{0} & \mathbf{0} & \mathbf{D}_2^{(3)} \end{bmatrix},$$

$$\mathbf{P} = \begin{bmatrix} \mathbf{P}^{(1)} & \mathbf{0} & \mathbf{0} \\ \mathbf{0} & \mathbf{P}^{(2)} & \mathbf{0} \\ \mathbf{0} & \mathbf{0} & \mathbf{P}^{(3)} \end{bmatrix}, \quad \mathbf{Q} = \begin{bmatrix} \mathbf{Q}^{(1)} & \mathbf{0} & \mathbf{0} \\ \mathbf{0} & \mathbf{Q}^{(2)} & \mathbf{0} \\ \mathbf{0} & \mathbf{0} & \mathbf{Q}^{(3)} \end{bmatrix},$$

The space derivative $(a(x)^2 u_x)_x$ is approximated as

$$(3.9) \qquad \mathbf{D}_1 \mathbf{A}^2 \mathbf{D}_1 \mathbf{u} = \mathbf{P}^{-1} \mathbf{Q} \mathbf{A}^2 \mathbf{P}^{-1} \mathbf{Q} \mathbf{u}.$$

3.2. The BCs. The cable equations are coupled by the interface BCs [AN13]. These are added as penalty terms to the semi-discretized PDE:

(3.10)
$$\mathbf{A}\mathbf{u}_t = \mu \mathbf{D}_1 \mathbf{A}^2 \mathbf{D}_1 \mathbf{u} - \frac{1}{C_m} \mathbf{A}\mathbf{G}(t)\mathbf{u} + \frac{1}{C_m} \mathbf{A}\mathbf{f}(t) + \mathbf{p}_{\text{soma}}(\mathbf{u}) + \mathbf{p}_{\text{sealed}}(\mathbf{u}) + \mathbf{p}_{\text{junction}}(\mathbf{u}).$$

---

[1] If $\mathbf{A} = [A_{ij}]$ and $\mathbf{B} = [B_{ij}]$, the Hadamard product has entries $\mathbf{A} \odot \mathbf{B} = [A_{ij}B_{ij}]$.

- $\mathbf{p}_{\text{soma}}(\mathbf{u}) = [\mathbf{p}_{\text{soma}}^{(1)}(\mathbf{u}^{(1)}), \mathbf{0}, \mathbf{0}]^T$ is the penalty term associated with the soma BC (2.14) at $x = \mathcal{L}^{(1)}$:

$$
\mathbf{p}_{\text{soma}}^{(1)}\left(\mathbf{u}^{(1)}\right)
$$
$$
= -\frac{\mu}{\eta}(\mathbf{P}^{(1)})^{-1}\left(u_{tN^{(1)}}^{(1)} + \eta\left(a_{N^{(1)}}^{(1)}\right)^2 u_{xN^{(1)}}^{(1)} + \frac{1}{C_m}g_{N^{(1)}}(t)u_{N^{(1)}}^{(1)}\right)\mathbf{e}_{N^{(1)}+1}^{(1)}.
$$

  $\mathbf{e}_j^{(c)}$ denotes here the jth vector of the identity matrix of dimension $N^{(c)}+1$.

- $\mathbf{p}_{\text{sealed}}(\mathbf{u}) = [\mathbf{0}, \mathbf{p}_{\text{sealed}}^{(2)}(\mathbf{u}^{(2)}), \mathbf{p}_{\text{sealed}}^{(3)}(\mathbf{u}^{(3)})]^T$ is associated with the sealed BCs (2.15):

$$
\mathbf{p}_{\text{sealed}}^{(c)}\left(\mathbf{u}^{(c)}\right) = -\mu\left(a_{N^{(c)}}^{(c)}\right)^2\left(\mathbf{P}^{(c)}\right)^{-1}\left(u_{xN^{(c)}}^{(c)}\right)\mathbf{e}_{N^{(c)}+1}^{(c)},\ c=2,3.
$$

- $\mathbf{p}_{\text{junction}}(\mathbf{u}) = [\mathbf{p}_{\text{junction}}^{(1)}(\mathbf{u}^{(1)}), \mathbf{p}_{\text{junction}}^{(2)}(\mathbf{u}^{(2)})\, \mathbf{p}_{\text{junction}}^{(3)}(\mathbf{u}^{(3)})]^Ts$ is associated with the junction BCs (2.16)–(2.17) at $x = 0$:

$$
\mathbf{p}_{\text{junction}}^{(c)}\left(\mathbf{u}^{(c)}\right) = \frac{\mu}{3}\sum_{1\leq j\neq c\leq 3}\left(\mathbf{P}^{(c)}\right)^{-1}\left(\mathbf{D}_1^{(c)}\right)^T\mathbf{e}_1^{(c)}\left(a_0^{(c)}\right)^2\left(u_0^{(c)} - u_0^{(j)}\right)
$$
$$
+ \frac{\mu}{3}\sum_{j=1}^3\left(\mathbf{P}^{(c)}\right)^{-1}\mathbf{e}_1^{(c)}\left(a_0^{(j)}\right)^2 u_{x0}^{(j)},\ c=1,\ldots,3.
$$

Stability and accuracy properties of the semidiscrete summation by parts–simultaneous approximation term scheme associated with the model network have been established in [AN13].

PROPOSITION 2. *The summation by part–simultaneous approximation term scheme for solving the semidiscrete problem associated with the initial boundary value problem* (2.12), (2.14), (2.15), (2.16), *and* (2.17) *for the model network is energy stable.*

3.3. Equations for the gating variables. The ODEs for the gating variables can be specified at each discretization point $x_j^{(c)}$ leading to the following vector-valued ODEs:

$$
(3.11)\qquad\begin{cases}\mathbf{m}_t^{(c)} = \boldsymbol{\alpha}_m\left(\mathbf{u}^{(c)}\right)\odot\left(\mathbf{1}-\mathbf{m}^{(c)}\right) - \boldsymbol{\beta}_m\left(\mathbf{u}^{(c)}\right)\odot\mathbf{m}^{(c)},\\ \mathbf{h}_t^{(c)} = \boldsymbol{\alpha}_h\left(\mathbf{u}^{(c)}\right)\odot\left(\mathbf{1}-\mathbf{h}^{(c)}\right) - \boldsymbol{\beta}_h\left(\mathbf{u}^{(c)}\right)\odot\mathbf{h}^{(c)},\\ \mathbf{n}_t^{(c)} = \boldsymbol{\alpha}_n\left(\mathbf{u}^{(c)}\right)\odot\left(\mathbf{1}-\mathbf{n}^{(c)}\right) - \boldsymbol{\beta}_n\left(\mathbf{u}^{(c)}\right)\odot\mathbf{n}^{(c)},\end{cases}
$$

where

$$
(3.12)\qquad\boldsymbol{\alpha}_m\left(\mathbf{u}^{(c)}\right) = \left[\alpha_m\left(u_0^{(c)}\right),\ldots,\alpha_m\left(u_{N^{(c)}}^{(c)}\right)\right]^T.
$$

The other vectorial quantities are defined similarly.

4. Model reduction.

4.1. State approximation. For each cable c, assume that a set of $L^{(c)}$ modes $\{\boldsymbol{\phi}_l^{(c)}\}_{l=1}^{L^{(c)}}$ is provided. These modes are stored as columns of a reduced basis matrix

$$
(4.1)\qquad\boldsymbol{\Phi}^{(c)} = [\boldsymbol{\phi}_1^{(c)},\ldots,\boldsymbol{\phi}_{L^{(c)}}^{(c)}] = \begin{bmatrix}\phi_{01}^{(c)} & \cdots & \phi_{1L^{(c)}}^{(c)}\\ \vdots & & \vdots\\ \phi_{N^{(c)}1}^{(c)} & \cdots & \phi_{N^{(c)}L^{(c)}}^{(c)}\end{bmatrix}.
$$

The solution vector $\mathbf{u}^{(c)}(t)$ is then approximated as a linear combination of those modes using the ansatz

$$\mathbf{u}^{(c)}(t) \approx \mathbf{u}_R^{(c)}(t) = \sum_{l=1}^{L^{(c)}} \phi_l^{(c)} q_l^{(c)}(t) = \boldsymbol{\Phi}^{(c)} \mathbf{q}^{(c)}(t). \tag{4.2}$$

The coefficients $\{q_l^{(c)}\}_{l=1}^{L^{(c)}}$ are the generalized (reduced) coordinates associated with the modes $\{\phi_l^{(c)}\}_{l=1}^{L^{(c)}}$. They are stored in a vector

$$\mathbf{q}^{(c)}(t) = \begin{bmatrix} q_1^{(c)} \\ \vdots \\ q_{L^{(c)}}^{(c)} \end{bmatrix}. \tag{4.3}$$

The next step consists in assembling the approximation for the network of three cables. In block form, defining

$$\mathbf{u}_R = \begin{bmatrix} \mathbf{u}_R^{(1)} \\ \mathbf{u}_R^{(2)} \\ \mathbf{u}_R^{(3)} \end{bmatrix}, \quad \mathbf{q} = \begin{bmatrix} \mathbf{q}^{(1)} \\ \mathbf{q}^{(2)} \\ \mathbf{q}^{(3)} \end{bmatrix}, \quad \boldsymbol{\Phi} = \begin{bmatrix} \boldsymbol{\Phi}^{(1)} & \mathbf{0} & \mathbf{0} \\ \mathbf{0} & \boldsymbol{\Phi}^{(2)} & \mathbf{0} \\ \mathbf{0} & \mathbf{0} & \boldsymbol{\Phi}^{(3)} \end{bmatrix}, \tag{4.4}$$

(4.2) becomes

$$\mathbf{u}_R(t) = \boldsymbol{\Phi}\mathbf{q}(t). \tag{4.5}$$

$\boldsymbol{\Phi}$ is the reduced-order basis (ROB). The choice of ROB $\boldsymbol{\Phi}$ will be specified in section 5.

4.2. Galerkin projection. Approximating the discrete solution $\mathbf{u}(t)$ by inserting $\mathbf{u}_R(t) = \boldsymbol{\Phi}\mathbf{q}(t)$ in (3.2), and neglecting the BCs for now, a nonzero residual $\mathbf{r}(t)$ appears as

$$\mathbf{A}\mathbf{u}_{Rt} = \mu \mathbf{P}^{-1}\mathbf{Q}\mathbf{A}^2\mathbf{D}_1\mathbf{u}_R - \frac{1}{C_m}\mathbf{A}\mathbf{G}_R(t)\mathbf{u}_R + \frac{1}{C_m}\mathbf{A}\mathbf{f}_R(t) + \mathbf{r}(t), \tag{4.6}$$

where $\mathbf{G}_R(t)$ is computed as

$$\mathbf{G}_R(t) = g_1\mathbf{diag}\left((\mathbf{m}_R(t))^3 \odot \mathbf{h}_R(t)\right) + g_2\mathbf{diag}\left((\mathbf{n}_R(t))^4\right) + g_3\mathbf{I}, \tag{4.7}$$

and $(\mathbf{m}_R(t), \mathbf{h}_R(t), \mathbf{n}_R(t))$ are computed from the solution of (3.11) based on $\mathbf{u}_R(t)$ instead of $\mathbf{u}(t)$. Similarly, $\mathbf{f}_R(t)$ is computed as

$$\mathbf{f}_R(t) = g_1 E_1 \left(\mathbf{m}_R(t)\right)^3 \odot \mathbf{h}_R(t) + g_2 E_2 \left(\mathbf{n}_R(t)\right)^4 + g_3 E_3 \mathbf{1} - \mathbf{i}(t). \tag{4.8}$$

Remark. In general $\mathbf{G}_R(t) \neq \mathbf{G}(t)$ and $\mathbf{f}_R(t) \neq \mathbf{f}(t)$. The efficient model reduction of the nonlinear terms $\mathbf{G}_R(t)$ and $\mathbf{f}_R(t)$ will be addressed in section 6.

Premultiplying (4.6) by $\boldsymbol{\Phi}^T\mathbf{P}$ and imposing the condition

$$\boldsymbol{\Phi}^T\mathbf{P}\mathbf{r}(t) = \mathbf{0} \tag{4.9}$$

leads to the Galerkin approximation equation which is a set of $\sum_{c=1}^{N^{(c)}} L^{(c)}$ equations in terms of $\sum_{c=1}^{N^{(c)}} L^{(c)}$ unknowns:

$$\boldsymbol{\Phi}^T\mathbf{P}\mathbf{A}\mathbf{u}_{Rt} = \mu\boldsymbol{\Phi}^T\mathbf{Q}\mathbf{A}^2\mathbf{D}_1\mathbf{u}_R - \frac{1}{C_m}\boldsymbol{\Phi}^T\mathbf{P}\mathbf{A}\mathbf{G}_R(t)\mathbf{u}_R + \frac{1}{C_m}\boldsymbol{\Phi}^T\mathbf{P}\mathbf{A}\mathbf{f}_R(t). \tag{4.10}$$

4.3. Reduced-order equations for the model network. BCs, integrated as penalty terms, are now considered. Similarly as in (4.10), the Galerkin projection based on the ansatz $\mathbf{u}_R(t) = \mathbf{\Phi}\mathbf{q}(t)$ leads to the set of reduced coupled equations

$$(4.11) \qquad \mathbf{M}_r \frac{d\mathbf{q}}{dt}(t) = -(\mathbf{K}_r + \mathbf{C}_r(t))\mathbf{q}_r(t) + \mathbf{d}_r(t),$$

where

$$(4.12) \quad \mathbf{M}_r = \begin{bmatrix} \mathbf{M}_r^{(1)} & \mathbf{0} & \mathbf{0} \\ \mathbf{0} & \mathbf{M}_r^{(2)} & \mathbf{0} \\ \mathbf{0} & \mathbf{0} & \mathbf{M}_r^{(3)} \end{bmatrix}, \ \mathbf{K}_r = \begin{bmatrix} \mathbf{K}_r^{(1)} & \mathbf{K}_r^{(1,2)} & \mathbf{K}_r^{(1,3)} \\ \mathbf{K}_r^{(2,1)} & \mathbf{K}_r^{(2)} & \mathbf{K}_r^{(2,3)} \\ \mathbf{K}_r^{(3,1)} & \mathbf{K}_r^{(3,2)} & \mathbf{K}_r^{(3)} \end{bmatrix},$$

$$\mathbf{C}_r(t) = \begin{bmatrix} \mathbf{C}_r^{(1)}(t) & \mathbf{0} & \mathbf{0} \\ \mathbf{0} & \mathbf{C}_r^{(2)}(t) & \mathbf{0} \\ \mathbf{0} & \mathbf{0} & \mathbf{C}_r^{(3)}(t) \end{bmatrix},$$

and $\mathbf{d}_r(t) = \mathbf{\Phi}^T \mathbf{P} \mathbf{A} \mathbf{f}_R(t)$ with blocks

$$(4.13) \quad \mathbf{M}_r^{(1)} = \mathbf{\Phi}^{(1)T}\mathbf{P}^{(1)}\mathbf{A}^{(1)}\mathbf{\Phi}^{(1)} + \frac{\mu}{\eta}\mathbf{\Phi}^{(1)T}\mathbf{e}_{N^{(1)}+1}^{(1)}\mathbf{e}_{N^{(1)}+1}^{(1)}{}^T\mathbf{\Phi}^{(1)},$$

$$(4.14) \quad \mathbf{M}_r^{(c)} = \mathbf{\Phi}^{(c)T}\mathbf{P}^{(c)}\mathbf{A}^{(c)}\mathbf{\Phi}^{(c)}, \ \ c > 1,$$

$$(4.15) \quad \mathbf{K}_r^{(c)} = \mu\mathbf{\Phi}^{(c)T}\mathbf{D}_1^{(c)T}\mathbf{P}^{(c)}\left(\mathbf{A}^{(c)}\right)^2\mathbf{D}_1^{(c)}\mathbf{\Phi}^{(c)}$$

$$(4.16) \qquad + \frac{2\mu}{3}\left(a_0^{(c)}\right)^2\left(\mathbf{\Phi}^{(c)T}\mathbf{e}_0^{(c)}\mathbf{e}_0^{(c)T}\mathbf{D}_1^{(c)}\mathbf{\Phi}^{(c)} - \mathbf{\Phi}^{(c)T}\mathbf{D}_1^{(c)T}\mathbf{e}_0^{(c)}\mathbf{e}_0^{(c)T}\mathbf{\Phi}^{(c)}\right),$$

$$(4.17) \quad \mathbf{K}_r^{(c,j)} = \frac{\mu}{3}\left(\left(a_0^{(j)}\right)^2\mathbf{\Phi}^{(c)T}\mathbf{e}_0^{(c)}\mathbf{e}_0^{(c)T}\mathbf{D}_1^{(j)}\mathbf{\Phi}^{(j)} - \left(a_0^{(c)}\right)^2\mathbf{\Phi}^{(c)T}\mathbf{D}_1^{(c)T}\mathbf{e}_0^{(c)}\mathbf{e}_0^{(c)T}\mathbf{\Phi}^{(j)}\right),$$

$$(4.18) \quad \mathbf{C}_r^{(1)}(t) = \frac{1}{C_m}\mathbf{\Phi}^{(1)T}\mathbf{P}^{(1)}\mathbf{A}^{(1)}\mathbf{G}_R^{(1)}(t)\mathbf{\Phi}^{(1)}$$

$$(4.19) \qquad + \frac{\mu}{\eta C_m}\mathbf{\Phi}^{(1)T}\sqrt{\mathbf{G}_R^{(1)}(t)}\mathbf{e}_{N^{(1)}+1}^{(1)}\mathbf{e}_{N^{(1)}+1}^{(1)}{}^T\sqrt{\mathbf{G}_R^{(1)}(t)}\mathbf{\Phi}^{(1)},$$

$$(4.20) \quad \mathbf{C}_r^{(c)}(t) = \frac{1}{C_m}\mathbf{\Phi}^{(c)T}\mathbf{P}^{(c)}\mathbf{A}^{(c)}\mathbf{G}_R^{(c)}(t)\mathbf{\Phi}^{(c)}, \ \ c = 2, 3.$$

The derivations of (4.11), (4.12), and (4.13)–(4.20) can be found in Appendix B.

4.4. Energy stability. To prove stability of the reduced system (4.11) (see [AN13]), the following weighted norm is defined for a given vector $\mathbf{u}$,

$$(4.21) \qquad \|\mathbf{u}\|_\star^2 = \left\|\sqrt{\mathbf{A}}\mathbf{u}\right\|^2 + \frac{\mu}{\eta}\left(u_{N^{(1)}}^{(1)}\right)^2 = \sum_{c=1}^3\left\|\sqrt{\mathbf{A}^{(c)}}\mathbf{u}^{(c)}\right\|^2 + \frac{\mu}{\eta}\left(u_{N^{(1)}}^{(1)}\right)^2.$$

In the remainder of this document, $\|\ \|$ denotes the vectorial or matrix norm induced by the matrix $\mathbf{P}$. Hence $\|\mathbf{v}\| = \sqrt{\mathbf{v}^T\mathbf{P}\mathbf{v}}$ and $\|\mathbf{M}\| = \sqrt{\mathrm{trace}(\mathbf{M}^T\mathbf{P}\mathbf{M})}$. Then, the following energy estimate holds, leading to Proposition 3,

$$(4.22) \qquad \left(\|\mathbf{u}_R\|_\star^2\right)_t + 2\mu\left\|\sqrt{\mathbf{A}}\mathbf{D}_1\mathbf{u}_R\right\|^2 + 2\left\|\sqrt{\frac{\mathbf{G}_R(t)}{C_m}}\mathbf{u}_R\right\|_\star^2 = 0.$$

PROPOSITION 3. *The scheme* (4.11) *for solving the reduced-order semidiscrete problem associated with the network depicted in Figure* 1 *is energy stable* [GKO95, NS05].

A proof is provided in Appendix C.

Remark. The advantage of writing a distinct ROM ansatz $\mathbf{u}_R^{(c)}(t) = \mathbf{\Phi}^{(c)}\mathbf{q}^{(c)}(t)$ for each cable $c = 1, \ldots, N_c$ is that it naturally leads to a stability result and an energy estimate identical to the one for its high-dimensional counterpart derived in [AN13]. This is a structure-preserving approach.

Remark. The energy estimate is here provided in terms of the $\| \|_\star$-norm which is the natural norm for the problem and finite differences discretization at hand. For a single cable, the l_2-norm $\| \|_2$ can be subsequently bounded in terms of the $\| \|_\star$-norm as

$$(4.23) \qquad \|\mathbf{u}_R\|_2 \leq \frac{1}{\min_{x \in [0,L]} a(x)} \|\mathbf{u}_R\|_\star.$$

5. ROB construction.

5.1. Single branch. A ROB is constructed by proper orthogonal decomposition (POD) based on snapshots [Sir87]. POD is the method of choice for constructing a ROB for nonlinear differential equations [CS10, AZF12, CFCA13]. It only requires collecting snapshots of the underlying high-dimensional model in an offline phase. Here, the POD basis is computed by simulation of the propagation of the potential in one branch. For that purpose, snapshots are generated from two distinct simulations, following [KCSC10]:

1. by simulating the propagation of an action potential from $x = 0$ to $x = \mathcal{L}$ by injecting a current at $x = 0$;
2. by simulating the propagation of an action potential from $x = \mathcal{L}$ to $x = 0$ by injecting a current at $x = \mathcal{L}$.

The corresponding N_s snapshots are then stored in a snapshot matrix $\overline{\mathbf{S}} \in \mathbb{R}^{(N^{(1)}-1) \times N_s}$ after removing the first and last entries corresponding to the boundary terms. In the following the notation $\overline{\mathbf{M}}$ denotes the matrix obtained by removing the first and last rows of a matrix $\mathbf{M}$.

A $\overline{\mathbf{P}}$-orthogonal ROB $\mathbf{\Phi}_c \in \mathbb{R}^{(N^{(1)}+1) \times L}$ of dimension $L > 2$ is then constructed by a singular value decomposition of $\overline{\mathbf{S}}$ as follows:

- Compute a truncated singular value decomposition of $\overline{\mathbf{P}}^{\frac{1}{2}}\overline{\mathbf{S}}$ of dimension $L-2$,

$$(5.1) \qquad \overline{\mathbf{P}}^{\frac{1}{2}}\overline{\mathbf{S}} \approx \overline{\mathbf{U}\mathbf{\Sigma}\mathbf{V}}^T.$$

- Let $\overline{\mathbf{\Phi}}_c = \overline{\mathbf{P}}^{-\frac{1}{2}}\overline{\mathbf{U}}$.

It can be shown that the ROB $\overline{\mathbf{\Phi}}_c$ of a given dimension $L - 2$ is optimal in the sense that it minimizes the following projection error of the snapshots:

$$(5.2) \qquad \mathcal{E}_{\text{proj}}(L - 2) = \frac{\left\|\overline{\mathbf{S}} - \overline{\mathbf{\Phi}}_c\overline{\mathbf{\Phi}}_c^T\overline{\mathbf{P}\mathbf{S}}\right\|}{\left\|\overline{\mathbf{S}}\right\|}$$

under constraints $\overline{\mathbf{\Phi}}_c^T\overline{\mathbf{P}\mathbf{\Phi}}_c = \mathbf{I}$.

Two extra basis vectors are then added to take into account the boundary degrees of freedom: these two vectors are the canonical basis vectors $\mathbf{e}_1 \in \mathbb{R}^{N^{(1)}+1}$ and $\mathbf{e}_{N+1} \in$

$\mathbb{R}^{N^{(1)}+1}$ associated with the two boundaries $x = 0$ and $x = \mathcal{L}$. A ROB $\mathbf{\Phi}_c$ including the BCs is finally constructed as

$$(5.3) \qquad \mathbf{\Phi}_c = \begin{bmatrix} 1 & 0 & \mathbf{0} \\ \mathbf{0} & \mathbf{0} & \overline{\mathbf{\Phi}}_c \\ 0 & 1 & \mathbf{0} \end{bmatrix} \in \mathbb{R}^{(N^{(1)}+1)\times L}.$$

Adding the two canonical vectors enables the exact enforcement of potential continuity at the boundaries of each cable when solving the reduced system of equations.

5.2. Entire network. The next step consists in assembling multiple cables into a network. In this work, for simplicity, the assumption of identical cables is considered. This means that the lengths of the cables are identical: $\mathcal{L}^{(c)} = \mathcal{L}$ and $N^{(c)} = N$. Further work will focus on tackling the case of different cables by following the parametric model reduction approaches developed in [AF08, ACCF09, AF11, PDTA15]. In the case of N_c identical cables, a ROB for the entire network can be constructed by blocks as

$$(5.4) \qquad \mathbf{\Phi} = \begin{bmatrix} \mathbf{\Phi}_c & & (\mathbf{0}) \\ & \ddots & \\ (\mathbf{0}) & & \mathbf{\Phi}_c \end{bmatrix} \in \mathbb{R}^{N_c(N+1)\times(N_c L)}.$$

The block structure of the ROB $\mathbf{\Phi}$ allows a flexible structure-preserving model reduction approach with an independent approximation in each cable. In turn, energy stability and accuracy properties follow from this block structure. Another advantage is that, after constructing a single cable ROB, a ROB can be constructed for any network topology by assembling a global ROB following the network structure.

6. Reduction of the time varying terms.

6.1. An issue with the evaluation of the gating functions. Computing the diagonal matrix $\mathbf{G}_R(t)$ at every time t is computationally expensive as it requires first computing $(\mathbf{m}_R(t), \mathbf{h}_R(t), \mathbf{n}_R(t))$ before constructing $\mathbf{G}_R(t)$ by (4.7) and then computing $\mathbf{C}_r(t)$ by (4.13)–(4.20). There is a similar complexity associated with constructing $\mathbf{f}_R(t)$ by (4.8). All of these steps are characterized by a computational complexity that scales with the large dimension $\sum_{c=1}^{N_c} N^{(c)}$ of the network.

To alleviate this computational burden that defeats the purpose of using a reduced-oder model, an additional reduction step is necessary to compute $\mathbf{G}_R(t)$ and $\mathbf{f}_R(t)$. That procedure is developed in the following section.

6.2. Efficient reduction of the time varying terms. In order to preserve the structure and energy stability properties of the equations of interest, a nonnegative variant of the discrete empirical interpolation method (DEIM) [CS10]—which itself is a discrete version of the EIM [BMNP04]—is developed in this work. It relies on the definition of two nonnegative ROBs to efficiently approximate the terms $\mathbf{G}_R(t)$ and $\mathbf{f}_R(t)$. It will be shown that this procedure preserves the energy stability of the underlying high-dimensional model.

The proposed approach proceeds by efficiently approximating the following two terms,

$$(6.1) \qquad \mathbf{m}(t)^3 \odot \mathbf{h}(t) \text{ and } \mathbf{n}(t)^4.$$

As proved in [AN13], the vectors $\mathbf{m}(t)$, $\mathbf{n}(t)$ and $\mathbf{h}(t)$ have all nonnegative entries.

Therefore, the terms $\mathbf{m}(t)^3 \odot \mathbf{h}(t)$ and $\mathbf{n}(t)^4$ are approximated by a nonnegative DEIM (NNDEIM) that preserves their positivity as follows.

1. Snapshots of the two nonnegative terms $\mathbf{m}(t)^3 \odot \mathbf{h}(t)$ and $\mathbf{n}(t)^4$ are first collected from a single branch and stored as columns of two respective snapshots matrices

   (6.2)
   $$\mathbf{N}_1 = [\mathbf{m}(t_1)^3 \odot \mathbf{h}(t_1), \ldots, \mathbf{m}(t_N)^3 \odot \mathbf{h}(t_N)] \text{ and } \mathbf{N}_2 = [\mathbf{n}(t_1)^4, \ldots, \mathbf{n}(t_N)^4].$$

2. Two nonnegative ROBs $\widehat{\mathbf{\Psi}}_1^{(c)}$ and $\widehat{\mathbf{\Psi}}_2^{(c)} \in \mathbb{R}^{(N^{(c)}+1) \times p}$ of dimension p are constructed from their respective snapshot matrices $\mathbf{N}_1$ and $\mathbf{N}_2$ and the nonnegative terms are approximated as

   (6.3) $$\mathbf{m}(t)^3 \odot \mathbf{h}(t) \approx \widehat{\mathbf{\Psi}}_1^{(c)} \mathbf{p}_1^{(c)}(t), \quad \mathbf{n}(t)^4 \approx \widehat{\mathbf{\Psi}}_2^{(c)} \mathbf{p}_2^{(c)}(t),$$

   where $\mathbf{p}_1^{(c)}(t)$ and $\mathbf{p}_2^{(c)}(t) \in \mathbb{R}^p$ are reduced coordinates whose computation is specified below.
   For the model network with three branches, the bases $\widehat{\mathbf{\Psi}}_1$ and $\widehat{\mathbf{\Psi}}_2$ are block diagonal and the reduced vectors $\mathbf{p}_1(t)$ and $\mathbf{p}_2(t)$ can be written as

   (6.4) $$\widehat{\mathbf{\Psi}}_j = \begin{bmatrix} \widehat{\mathbf{\Psi}}_j^{(1)} & \mathbf{0} & \mathbf{0} \\ \mathbf{0} & \widehat{\mathbf{\Psi}}_j^{(2)} & \mathbf{0} \\ \mathbf{0} & \mathbf{0} & \widehat{\mathbf{\Psi}}_j^{(3)} \end{bmatrix}, \quad \mathbf{p}_j(t) = \begin{bmatrix} \mathbf{p}_j^{(1)}(t) \\ \mathbf{p}_j^{(2)}(t) \\ \mathbf{p}_j^{(3)}(t) \end{bmatrix}, \quad j = 1, 2.$$

3. A reduced mask $\mathbf{Z}$ constituted of p columns of the identity matrix is then selected by a modified version of the greedy algorithm of [CS10], as developed in [CBMF11, CFCA13] and described in Appendix D. The reduced coordinates $\mathbf{p}(t)$ are then computed by matching the corresponding entries of the nonlinear term either exactly or in the least-squares sense as solutions of two nonnegative least-squares problems

   (6.5) $$\mathbf{p}_1(t) = \underset{\mathbf{q} \geq \mathbf{0}}{\operatorname{argmin}} \left\| \left(\mathbf{Z}^T \widehat{\mathbf{\Psi}}_1 \right) \mathbf{q} - \mathbf{Z}^T \left(\mathbf{m}(t)^3 \odot \mathbf{h}(t) \right) \right\|_2,$$

   (6.6) $$\mathbf{p}_2(t) = \underset{\mathbf{q} \geq \mathbf{0}}{\operatorname{argmin}} \left\| \left(\mathbf{Z}^T \widehat{\mathbf{\Psi}}_2 \right) \mathbf{q} - \mathbf{Z}^T \left(\mathbf{n}(t)^4 \right) \right\|_2.$$

   The nonnegative ROBs $\widehat{\mathbf{\Psi}}_j = [\widehat{\psi}_{j1}, \ldots, \widehat{\psi}_{jp}]$ are constructed by one of the following methods:
   - by nonnegative matrix factorization (NNMF) [LS99, KHP13] of the form

     (6.7) $$\mathbf{N}_j \approx \widehat{\mathbf{\Psi}}_j \mathbf{H}_j, \quad \widehat{\mathbf{\Psi}}_j \geq \mathbf{0}, \quad \mathbf{H}_j \geq \mathbf{0}.$$

     The advantage of this approach is that a black-box NNMF computation toolbox such as the one developed in [KP08] can be readily used to compute the ROBs $\widehat{\mathbf{\Psi}}_1$ and $\widehat{\mathbf{\Psi}}_2$. The disadvantage of NNMF is that no closed-form solution to the low-rank nonnegative factorization problem exists. Hence, there is no guarantee that the ROBs that are computed are optimal;

- by a dictionary approach in which the columns of $\widehat{\mathbf{\Psi}}_j$ are chosen among columns of $\mathbf{N}_j$ in a greedy fashion. The first vector is chosen to be the column of snapshot with largest magnitude and at each subsequent step of the greedy procedure, the column with the largest error associated with the current basis is selected and the basis is extended with that vector. That procedure is described in Algorithm 1.

Algorithm 1 Greedy construction of a nonnegative ROB $\widehat{\mathbf{\Psi}}_j$

Require: Snapshot matrix $\mathbf{N}_j$
Ensure: Nonnegative ROB $\widehat{\mathbf{\Psi}}_j$ and mask matrix $\mathbf{Z}$
1: Find the index i_0 of the column of $\mathbf{N}_j = [\mathbf{n}_1, \ldots, \mathbf{n}_M]$ with largest magnitude and let
$$\widehat{\mathbf{\Psi}}_j = \mathbf{n}_{i_0}$$

2: Compute $\mathbf{Z}$ by Algorithm 2 (see Appendix E)
3: **for** $i = 2, \ldots, p$ **do**
4:   Find the snapshot $\mathbf{n}_{i_0}$ with largest reconstruction error
$$i_0 = \underset{i=1\ldots,M}{\operatorname{argmax}} \frac{\|\widehat{\mathbf{\Psi}}_j \mathbf{p}_j - \mathbf{n}_i\|_2}{\|\mathbf{n}_i\|_2}$$

5:   Add $\mathbf{n}_{i_0}$ to the ROB
$$\widehat{\mathbf{\Psi}}_j = [\widehat{\mathbf{\Psi}}_j, \mathbf{n}_{i_0}]$$

6:   Compute $\mathbf{Z}$ by Algorithm 2
7: **end for**

---

4. In practice, the diagonal matrix $\mathbf{G}_R(t)$ is approximated as

$$(6.8) \qquad \mathbf{G}_R(t) \approx \widehat{\mathbf{G}}_R(t) = g_1 \mathbf{diag}\left(\widehat{\mathbf{\Psi}}_1 \mathbf{p}_1(t)\right) + g_2 \mathbf{diag}\left(\widehat{\mathbf{\Psi}}_2 \mathbf{p}_2(t)\right) + g_3 \mathbf{I}.$$

Similarly,

$$(6.9) \quad \mathbf{f}_R(t) \approx \widehat{\mathbf{f}}_R(t) = g_1 E_1\left(\widehat{\mathbf{\Psi}}_1 \mathbf{p}_1(t)\right) + g_2 E_2\left(\widehat{\mathbf{\Psi}}_2 \mathbf{p}_2(t)\right) + g_3 E_3 \mathbf{1} - \mathbf{i}(t).$$

5. The reduced-order equations (4.11) are then approximated as

$$(6.10) \qquad \mathbf{M}_r \frac{d\mathbf{q}}{dt}(t) = -\left(\mathbf{K}_r + \widehat{\mathbf{C}}_r(t)\right) \mathbf{q}(t) + \widehat{\mathbf{d}}_r(t),$$

leading to a solution $\widehat{\mathbf{u}}_R(t) = \mathbf{\Phi}\mathbf{q}(t)$ of the reduced system with a time varying terms approximation. $\widehat{\mathbf{d}}_r(t) = \mathbf{\Phi}^T \mathbf{P} \mathbf{A} \widehat{\mathbf{f}}_R(t)$ and

$$(6.11) \qquad \widehat{\mathbf{C}}_r(t) = \begin{bmatrix} \widehat{\mathbf{C}}_r^{(1)}(t) & \mathbf{0} & \mathbf{0} \\ \mathbf{0} & \widehat{\mathbf{C}}_r^{(2)}(t) & \mathbf{0} \\ \mathbf{0} & \mathbf{0} & \widehat{\mathbf{C}}_r^{(3)}(t) \end{bmatrix}$$

with

$$(6.12) \quad \widehat{\mathbf{C}}_r^{(1)}(t) = \frac{1}{C_m} \boldsymbol{\Phi}^{(1)^T} \mathbf{P}^{(1)} \mathbf{A}^{(1)} \widehat{\mathbf{G}}_R^{(1)}(t) \boldsymbol{\Phi}^{(1)}$$

$$(6.13) \qquad + \frac{\mu}{\eta C_m} \boldsymbol{\Phi}^{(1)^T} \sqrt{\widehat{\mathbf{G}}_R^{(1)}(t)} \mathbf{e}_{N^{(1)}+1}^{(1)} \mathbf{e}_{N^{(1)}+1}^{(1)^T} \sqrt{\widehat{\mathbf{G}}_R^{(1)}(t)} \boldsymbol{\Phi}^{(1)},$$

$$(6.14) \quad \widehat{\mathbf{C}}_r^{(c)}(t) = \frac{1}{C_m} \boldsymbol{\Phi}^{(c)^T} \mathbf{P}^{(c)} \mathbf{A}^{(c)} \widehat{\mathbf{G}}_R^{(c)}(t) \boldsymbol{\Phi}^{(c)}, \quad c > 1.$$

The operators $\widehat{\mathbf{C}}_r^{(c)}(t)$ and $\widehat{\mathbf{d}}_r(t)$ can be efficiently evaluated when solving the ODE (4.11) online by noticing that precomputations of certain constant terms can be done once for all offline. For instance, the term $\widehat{\mathbf{C}}_r^{(c)}(t)$, $c > 1$, can be written as

$$\widehat{\mathbf{C}}_r^{(c)}(t) = \sum_{i=1}^p \left(\frac{g_1}{C_m} \boldsymbol{\Phi}^{(c)^T} \mathbf{P}^{(c)} \mathbf{A}^{(c)} \mathbf{diag}\left(\widehat{\psi}_{1i}\right) \boldsymbol{\Phi}^{(c)} \right) p_{1i}(t)$$

$$+ \sum_{i=1}^p \left(\frac{g_2}{C_m} \boldsymbol{\Phi}^{(c)^T} \mathbf{P}^{(c)} \mathbf{A}^{(c)} \mathbf{diag}\left(\widehat{\psi}_{2i}\right) \boldsymbol{\Phi}^{(c)} \right) p_{2i}(t)$$

$$+ \left(\frac{g_3}{C_m} \boldsymbol{\Phi}^{(c)^T} \mathbf{P}^{(c)} \mathbf{A}^{(c)} \boldsymbol{\Phi}^{(c)} \right)$$

$$= \sum_{i=1}^p \left(\widehat{\mathbf{J}}_{i,1}^{(c)} p_{1i}(t) + \widehat{\mathbf{J}}_{i,2}^{(c)} p_{2i}(t) \right) + \widehat{\mathbf{J}}_0^{(c)}.$$

Hence, the operator $\widehat{\mathbf{C}}_r^{(c)}(t)$ can be efficiently evaluated by precomputing once for all the following small size operators of dimension L before solving (4.11):

$$\widehat{\mathbf{J}}_{i,1}^{(c)} = \frac{g_1}{C_m} \boldsymbol{\Phi}^{(c)^T} \mathbf{P}^{(c)} \mathbf{A}^{(c)} \mathbf{diag}\left(\widehat{\psi}_{1i}\right) \boldsymbol{\Phi}^{(c)}, \ i = 1, \ldots, p,$$

$$\widehat{\mathbf{J}}_{i,2}^{(c)} = \frac{g_2}{C_m} \boldsymbol{\Phi}^{(c)^T} \mathbf{P}^{(c)} \mathbf{A}^{(c)} \mathbf{diag}\left(\widehat{\psi}_{2i}\right) \boldsymbol{\Phi}^{(c)}, \ i = 1, \ldots, p,$$

$$\widehat{\mathbf{J}}_0^{(c)} = \frac{g_3}{C_m} \boldsymbol{\Phi}^{(c)^T} \mathbf{P}^{(c)} \mathbf{A}^{(c)} \boldsymbol{\Phi}^{(c)}.$$

The terms $\widehat{\mathbf{C}}_r^{(1)}(t)$ and $\widehat{\mathbf{d}}_r(t)$ can be also evaluated efficiently online by precomputing similar terms.

A comparison of (6.10)–(6.14) with (4.11)–(4.20) shows that the proposed reduction approach preserves the fundamental structure of the equations. Furthermore, the following energy stability result can be proved. Its proof is analogous to the one of Proposition 3.

PROPOSITION 4. *The following energy estimate*

$$(6.15) \qquad \left(\|\widehat{\mathbf{u}}_R\|_\star^2 \right)_t + 2\mu \left\| \sqrt{\mathbf{A}} \mathbf{D}_1 \widehat{\mathbf{u}}_R \right\|^2 + 2 \left\| \sqrt{\frac{\widehat{\mathbf{G}}_R(t)}{C_m}} \widehat{\mathbf{u}}_R \right\|_\star^2 = 0$$

and hence the scheme (6.10) *based on NNDEIM is energy stable* [GKO95, NS05].

7. A posteriori error estimation.

7.1. Galerkin projection. An a posteriori error estimate is first derived for the case of the model network connected to the soma.

PROPOSITION 5. *Consider the case of the model network connected to the soma. Let* $\mathbf{u}_R(t) = \mathbf{\Phi}\mathbf{q}(t)$ *denote the solution to the reduced-order system and* $\mathbf{u}(t)$ *the solution to its full-order counterpart. The error* $\mathbf{e}(T) = \mathbf{u}_R(T) - \mathbf{u}(T)$ *at a given time* $T > 0$ *satisfies the inequality*

$$(7.1) \qquad \|\mathbf{e}(T)\|_\star \leq \|\mathbf{e}(0)\|_\star e^{-\delta_0 T} + \frac{1}{\min_i \sqrt{a_i}} \frac{1 - e^{-\delta_0 T}}{\delta_0} \sup_{t \in [0,T]} B(t),$$

where

$$(7.2) \qquad B(t) = \|\mathbf{r}(t)\| + C_G \|\mathbf{G}_R(t) - \mathbf{G}(t)\|_2 \|\mathbf{u}_R(t)\|_2 + C_f \|\mathbf{f}_R(t) - \mathbf{f}(t)\|_2$$

and $C_f = \frac{\|\mathbf{A}\|}{C_m}$, $C_G = C_f(1 + \frac{\mu}{\eta})$, $\delta_0 = \frac{g_{\min}}{C_m}$. $\mathbf{r}(t)$ *denotes the residual*

$$(7.3) \qquad \begin{aligned} \mathbf{r}(t) = \mathbf{A}\mathbf{u}_{Rt} - \mu \mathbf{D}_1 \mathbf{A}^2 \mathbf{D}_1 \mathbf{u}_R + \frac{1}{C_m}\mathbf{A}\mathbf{G}_R(t)\mathbf{u}_R - \frac{1}{C_m}\mathbf{A}\mathbf{f}_R(t) \\ - \mathbf{p}_{soma}(\mathbf{u}_R) - \mathbf{p}_{sealed}(\mathbf{u}_R) - \mathbf{p}_{junction}(\mathbf{u}_R). \end{aligned}$$

This error bound is proved in Appendix E.

Remark. As the dimension of the ROB $\mathbf{\Phi}$ increases, in practice, the residual $\|\mathbf{r}(t)\|$ and the differences $\|\mathbf{G}(t) - \mathbf{G}_R(t)\|_2$ and $\|\mathbf{f}_R(t) - \mathbf{f}(t)\|_2$ decrease. These two differences are in practice bounded, leading to the following bound
(7.4)
$$\|\mathbf{e}(T)\|_\star \leq \|\mathbf{e}(0)\|_\star e^{-\delta_0 T} + \frac{1}{\min_i \sqrt{a_i}} \sup_{t \in [0,T]} \left(\|\mathbf{r}(t)\| + C_G'\|\mathbf{u}_R(t)\|_2 + C_f' \right) \frac{1 - e^{-\delta_0 T}}{\delta_0},$$

where $C_G' = (g_1 + g_2)C_G$ and $C_f' = (g_1|E_1| + g_2|E_2|)\sum_{c=1}^{N_c}(N^{(c)} + 1)C_f$

Proof. $g_3 \leq g_j^{(c)}, g_{Rj}^{(c)} \leq \sum_{i=1}^3 g_i$ (see [AN13]). Hence $|g_j^{(c)} - g_{Rj}^{(c)}| \leq g_1 + g_2$ and $\|\mathbf{G}_R - \mathbf{G}\|_2 \leq g_1 + g_2$. Similarly, $|f_j^{(c)} - f_{Rj}^{(c)}| \leq g_1|E_1| + g_2|E_2|$ and therefore $\|\mathbf{f}_R - \mathbf{f}\|_2 \leq (g_1|E_1| + g_2|E_2|)\sum_{c=1}^{N_c}(N^{(c)} + 1)$.

Note that the a posteriori error bound (7.4) can be readily estimated by plugging the solution $\mathbf{u}_R(t)$ of the reduced system (4.11) and the associated residual $\mathbf{r}(t)$. It does not require the unknown quantities $\mathbf{G}(t)$ and $\mathbf{f}(t)$ associated with the solution of the high-dimensional model. ☐

7.2. Nonnegative discrete empirical interpolation. A posteriori error estimates are now derived for ROMs with NNDEIM.

PROPOSITION 6. *Consider the case of a model network connected to the soma. The error* $\widehat{\mathbf{e}}(T) = \widehat{\mathbf{u}}_R(T) - \mathbf{u}(T)$ *at a given time* $T > 0$ *satisfies the inequalities*

$$(7.5) \qquad \|\widehat{\mathbf{e}}(T)\|_\star \leq \|\widehat{\mathbf{e}}(0)\|_\star e^{-\delta_0 T} + \frac{1 - e^{-\delta_0 T}}{\delta_0} \frac{1}{\min_i \sqrt{a_i}} \sup_{t \in [0,T]} \widehat{B}(t)$$

with

$$(7.6) \qquad \widehat{B}(t) = \|\widehat{\mathbf{r}}(t)\| + C_G \|\widehat{\mathbf{G}}_R(t) - \mathbf{G}(t)\|_2 \|\widehat{\mathbf{u}}_R(t)\|_2 + C_f \|\widehat{\mathbf{f}}_R(t) - \mathbf{f}(t)\|_2,$$

and

$$(7.7) \qquad \|\widehat{\mathbf{e}}(T)\|_\star \leq \|\widehat{\mathbf{e}}(0)\|_\star e^{-\delta_0 T} + \frac{1 - e^{-\delta_0 T}}{\delta_0} \frac{1}{\min_i \sqrt{a_i}} \sup_{t \in [0,T]} \widehat{B}'(t)$$

with

$$(7.8) \qquad \widehat{B}'(t) = \|\widehat{\mathbf{r}}(t)\| + \sum_{j=1}^{2} g_j \left(1 + \frac{2n_c \|\widehat{\boldsymbol{\Psi}}_j\|_2}{\sigma_{\min}(\mathbf{Z}^T \widehat{\boldsymbol{\Psi}}_j)} \right) (C_G \|\widehat{\mathbf{u}}_R(t)\|_2 + C_f |E_j|),$$

and $\sigma_{\min}(\mathbf{M})$ denotes the smallest singular value of a matrix $\mathbf{M}$ and $\widehat{\mathbf{r}}(t)$ denotes the residual obtained by substituting for $\mathbf{u}_R(t)$ by $\widehat{\mathbf{u}}_R(t)$ in (7.3).

This second estimate can be evaluated a posteriori based only on the solution $\widehat{\mathbf{u}}_R(t)$ as it does not involve the unknown quantities $\mathbf{G}(t)$ and $\mathbf{f}(t)$ associated with the solution of the high-dimensional model. A proof of this estimate is given in Appendix F.

The error estimators presented in this section are not expected to be tight. However, they illustrate the three contributions to the model reduction error: (1) state approximation resulting in a residual vector, (2) $\mathbf{G}$ function approximation from NNDEIM, and (3) $\mathbf{f}$ function approximation from NNDEIM. In order to obtain tighter error estimates, an extension of the approach developed in [AH15] to nonlinear models could be envisioned.

8. Numerical applications. In the numerical experiments, an ROM is first constructed for a single cable configuration. An extensive study is performed in section 8.1 to chose appropriate dimensions for that ROM. Furthermore, a comparison with an approach that does not enforce positivity of the matrix $\widehat{\mathbf{G}}_R$ is also compared to the proposed methodology.

In a second step, the ROM constructed for a single cable is used in section 8.2 for the fast simulation of an arbitrary network by assembling a series of such one-cable ROMs according to the network topology.

All experiments are performed with MATLAB R2013B running on a Mac Book Pro 3 GHz Intel Core i7, 16 GB 1600 MHz DDR3. We have uploaded the source code used to run the numerical experiments on the zenodo.org website.[2]

8.1. Cable with soma. In the first numerical experiment, the propagation of the action potential in a single cable connected to the soma is studied. The cable properties correspond to that of the giant squid. The cable diameter is constant and equal to 0.48 mm and its length is $\mathcal{L} = 5$ cm. All other physical properties and constants are described in detail in [AN13].

The domain $x \in [0, \mathcal{L}]$ is discretized using $N = 1000$ points. Fifth-order operators in space are used. Time integration is done using the Crank–Nicholson scheme presented in [AN13] with a time step of 10^{-5} s. 2000 snapshots are generated by computing the propagation of the action potential in the cable in two ways: (1) when the input current with maximum intensity 10^{-8} A is applied at $x = 0$ and the action potential propagates from 0 to $\mathcal{L}$; (2) when the input is applied at $x = \mathcal{L}$ and the action potential propagates from $\mathcal{L}$ to 0. Each of these high-dimensional model computations leads to a CPU time of 5.27 s.

The relative projection errors $\mathcal{E}_{\mathrm{proj}}(L)$ (as defined in (5.2)) associated with the snapshots are reported in Figure 2 for ROB sizes of dimension ranging from $L = 1$ to $L = 60$. For $L = 60$ the error $\mathcal{E}_{\mathrm{proj}}(L)$ is as low as 10^{-6} %.
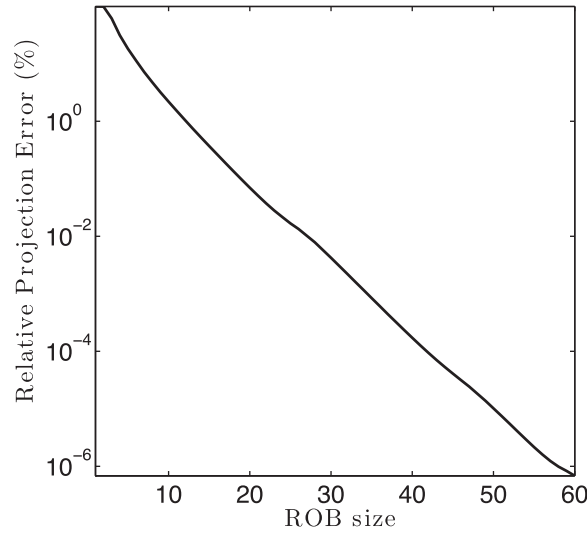
---

[2]https://zenodo.org/record/44950.

FIG. 2. *Snapshot projection error $\mathcal{E}_{proj}(L)$ associated with ROB size of varying dimension L.*
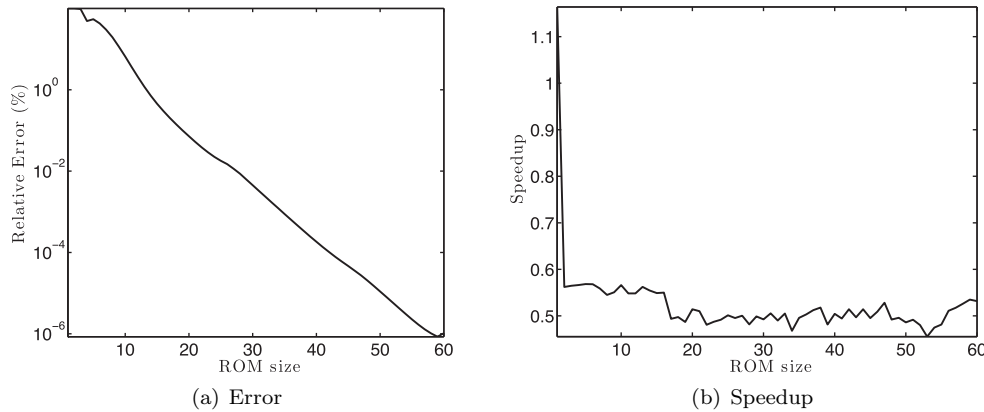

(a) Error

(b) Speedup

FIG. 3. *Relative errors and speedups associated with ROMs of various dimensions for one cable.*

The ROBs are then used to simulate the propagation of the potential in a single cable of length $\mathcal{L}$ connected to a soma when a synaptic input current is applied at the other extremity of the cable. The following relative error norm $\mathcal{E}_{\text{sol}}(L)$ associated with a ROM solution $\mathbf{u}_R$ computed with a ROB $\mathbf{\Phi}_c$ of dimension L is reported in Figure 3(a):

$$(8.1) \qquad \mathcal{E}_{\text{sol}}(L) = \left(\frac{\sum_{i=1}^{M} \|\mathbf{u}(t_i) - \mathbf{u}_R(t_i)\|^2}{\sum_{i=1}^{M} \|\mathbf{u}(t_i)\|^2} \right)^{\frac{1}{2}}.$$

By comparing the results to Figure 2, one can observe that, for the same ROB dimension L, the errors $\mathcal{E}_{\text{sol}}(L)$ and $\mathcal{E}_{\text{proj}}(L)$ are of the same order of magnitude. The relative error is less than 1 % for $L \geq 14$. Hence, in the remainder of this paper, a ROB $\mathbf{\Phi}_c$ of dimension $L = 15$ will be chosen.

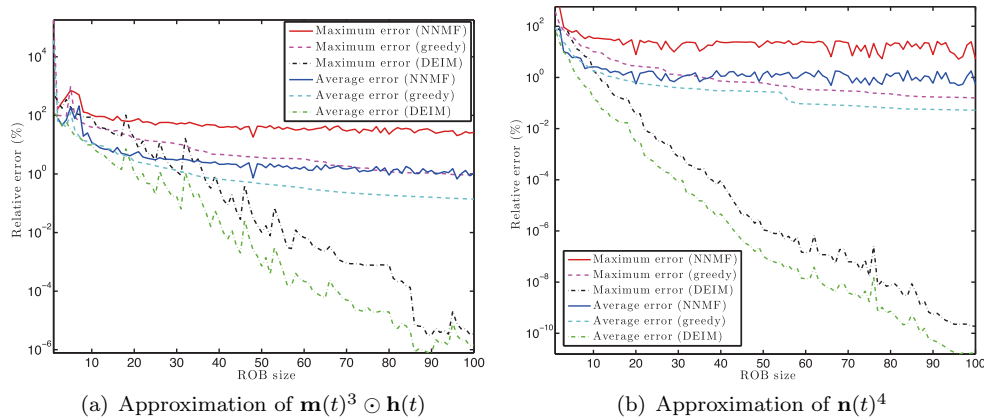(a) Approximation of $\mathbf{m}(t)^3 \odot \mathbf{h}(t)$ (b) Approximation of $\mathbf{n}(t)^4$

FIG. 4. *Relative errors of the snapshots reconstruction by NNDEIM using the two proposed nonnegative ROB construction approaches.*

The speedups are reported in Figure 3(b). One can observe that the speedup drops sharply for $L > 1$ and the speedup associated with a ROB of dimension $L = 15$ is only 0.55 which means that solving the ROM is actually more expensive than solving the underlying high-dimensional model.

To obtain speedups, the proposed NNDEIM-based approach is then pursued. Two reduced bases $\widehat{\mathbf{\Psi}}_1$ and $\widehat{\mathbf{\Psi}}_2$ are first constructed. As outlined in section 6.2, two methodologies are possible to construct those bases.

The first approach is based on NNMFs. For that purpose, a MATLAB implementation [KP08] based on alternative nonnegative least squares using block principal pivoting [KHP13] is considered, Reduced bases $\widehat{\mathbf{\Psi}}_1(p)$ and $\widehat{\mathbf{\Psi}}_2(p)$ are constructed for dimensions p varying from 1 to 100. For each dimension p of the ROBs a mask $\mathbf{Z}(p)$ of the same dimension is constructed by the greedy algorithm outlined in Appendix D. The relative errors incurred by the NNMF approach in reconstructing the snapshots vectors $\mathbf{n}_j(t_i)$ contained in $\mathbf{N}_j$, $j = 1, 2$, are then computed as

$$(8.2) \qquad \mathcal{E}_{\text{NNMF},ji}(p) = \frac{\|\widehat{\mathbf{\Psi}}_j(p)\mathbf{p}_j(t_i) - \mathbf{n}_j(t_i)\|_2}{\|\mathbf{n}_j(t_i)\|_2}$$

and the following maximum and average relative errors computed as

$$(8.3) \quad \mathcal{E}_{\text{NNMF},j,\text{max}}(p) = \max_{i=1,\ldots,M} \mathcal{E}_{\text{NNMF},ji}(p), \quad \mathcal{E}_{\text{NNMF},j,\text{avg}}(p) = \frac{1}{M}\sum_{i=1}^{M} \mathcal{E}_{\text{NNMF},ji}(p).$$

These errors are reported in Figure 4. One can observe that the approximation errors of $\mathbf{m}(t)^3 \odot \mathbf{h}(t)$ and $\mathbf{n}(t)$ drop sharply for increasing values of p until $p \approx 30$ for which the average errors are of the order of 1% and the maximum errors of the order of 20%

The second approach is based on the greedy procedure developed in Algorithm 1. Maximum and average relative errors $\mathcal{E}_{\text{greedy},j,\text{max}}(p)$ and $\mathcal{E}_{\text{greedy},j,\text{avg}}(p)$ defined similarly as in (8.3) are computed and reported in Figure 4. The errors of $\mathbf{m}(t)^3 \odot \mathbf{h}(t)$ and $\mathbf{n}(t)$ decrease sharply with increasing ROB size p. The errors are several order of magnitude smaller for the greedy approach when compared to NNMF. For instance, for $p = 100$ the average errors $\mathcal{E}_{\text{greedy},j,\text{avg}}(p)$ are of the order of 0.1% and the maximum errors $\mathcal{E}_{\text{greedy},j,\text{max}}(p)$ of the order 1% for $\mathbf{m}(t)^3 \odot \mathbf{h}(t)$ and 0.2% for $\mathbf{n}(t)$. The greedy
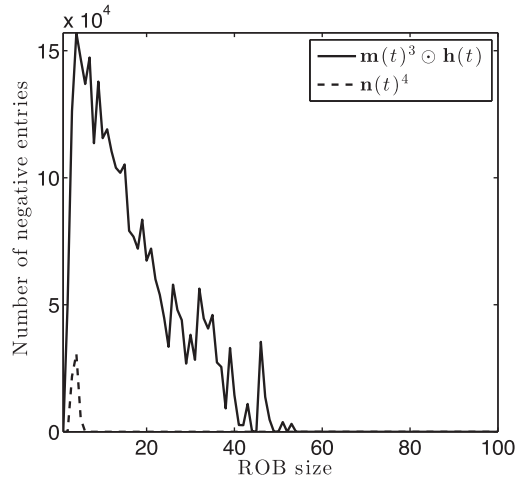
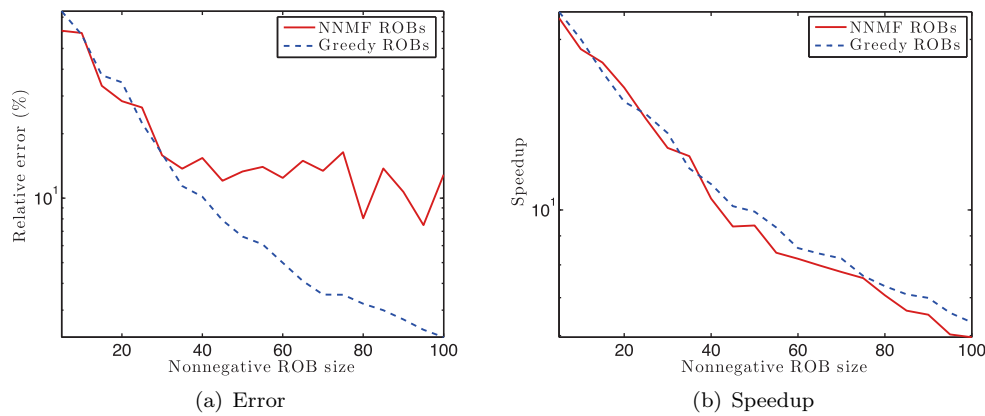FIG. 5. *Number of cumulated negative entries of the vectors reconstructed by DEIM.*

(a) Error   (b) Speedup

FIG. 6. *Relative errors and speedups associated with ROMs of various dimensions for one cable using the NNDEIM approximation.*

approach leads to much smaller errors, thanks to targeting in Algorithm 1 snapshots corresponding to the largest error at each iteration. In contrast, the NNMF-based approach does not take into account that error when the ROBs are constructed and the error stagnates after $p = 30$.

Finally, DEIM is applied to the same training set. One can observe from the results reported in Figure 4 that equivalent errors are obtained when $p \leq 10$. The errors in terms of approximation are several orders of magnitude lower with DEIM as a positive constraint on the approximation results in a suboptimal approximation error. However, as illustrated in Figure 5, many entries of the vectors resulting from the DEIM approximation are negative. Increasing the value of p reduces the number of such entries and all entries are positive for $p \geq 55$.

The two sets of nonnegative ROBs are then used to solved the reduced system (6.10) for dimensions p of the bases ranging from 5 to 100. The relative errors and speedups associated with these ROMs are reported in Figure 6. One can ob-
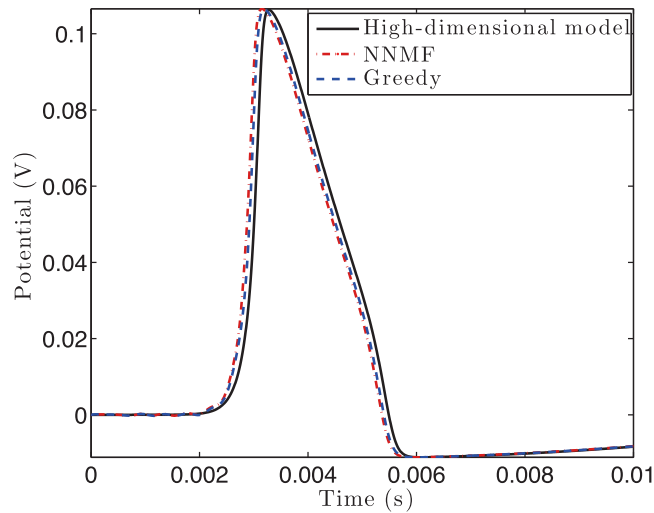
Fig. 7. *Comparison of the potential at the soma computed using the two NNDEIM approaches for p = 60.*

serve that the errors associated with the NNMF-based and greedy-based ROBs are comparable for $p \leq 35$. For $p \geq 35$ however, the relative error associated with the greedy-based ROBs continually decreases to a level of 2% for $p = 100$. However, the relative errors associated with the NNMF-based ROBs stagnates to a level of about 10%. As such, the greedy-based ROBs are preferred in the remainder of this work. The speedups are almost identical in both cases, ranging from about 22 for small ROBs to 7 for large ROBs. Compared with the speedups shown in Figure 3, this confirms that using additional approximations for the nonnegative terms enables important speedups.

The potentials recorded at the soma with each approach are shown in Figure 7. The results show that both approaches result in a potential that matches very well their high-dimensional counterpart. There is however a slight time delay between the reduced and high-dimensional responses.

Next, the importance of using nonnegative ROBs is showcased. The predictions associated with a ROM based on nonnegative ROBs constructed by the greedy method are compared with predictions that do not take into account the positivity of the terms $\mathbf{m}(t)^3 \odot \mathbf{h}$ and $\mathbf{n}(t)$. For that purpose the DEIM approach of [CS10] is directly applied to approximate those two terms. The results are compared in Figure 8. The ROM based on NNDEIM approximations lead to a physical potential response, albeit with a delay in the response when compared to the high-dimensional model. On the other hand, the ROM based on DEIM quickly becomes unstable and *not a number* (NaN) values are obtained for $t \approx 0.001$ s. This emphasizes that positivity of the two terms should be enforced. As demonstrated by the results in Figure 5, increasing p would at some point result in positivity and stability with DEIM. However, stability can only be determined a posteriori and only NNDEIM provides a theoretical guaranteed stability.

8.2. Network of cables. A network of 15 dendritic cables organized in four layers and attached to the soma is now considered. The network is depicted in Figure 9. The simulation of propagation in this network using a high-dimensional model leads to a CPU time of 10.4 minutes.
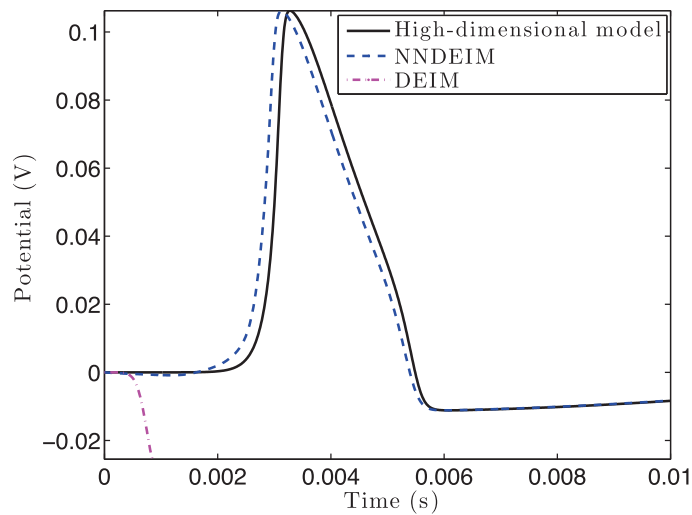
FIG. 8. *Comparison of the potential at the soma computed using the NNDEIM and DEIM approaches for $p = 5$.*
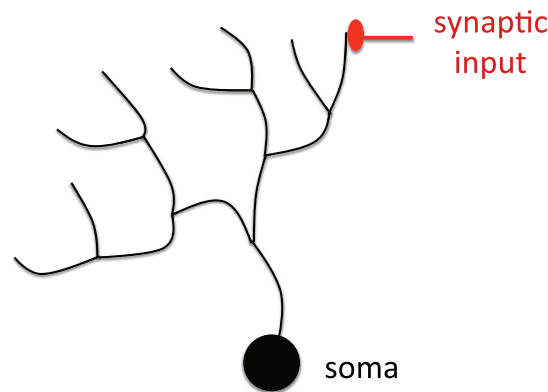

FIG. 9. *Large-scale network of 15 dendritic cables connected to a soma.*

The state ROB of dimension $L = 15$ together with the two nonnegative ROBs of dimension $p = 60$ constructed previously using the greedy approach are used to predict the potential variation at the soma. The results are reported in Figure 10. One can observe that the response has the appropriate amplitude, albeit with a slight shift in time. The speedup for that simulation is 20.1 which demonstrates the capability of the proposed approach to allow important speedups for simulating the potential propagation in large networks. On the other hand, the speedup obtained with Galerkin projection only is 1.3 which is insufficient.

9. Conclusions. A guaranteed energy stable model reduction approach for the fast simulation of potential propagation in large-scale neuronal networks is presented in this work. The approach preserves the structure of the high-dimensional approximation of the Hodgkin–Huxley equations while enabling important speedups. The structure of the system of equations is preserved by defining a distinct ROB for each cable in the network. Stability of the ROM model is guaranteed thanks to this struc-
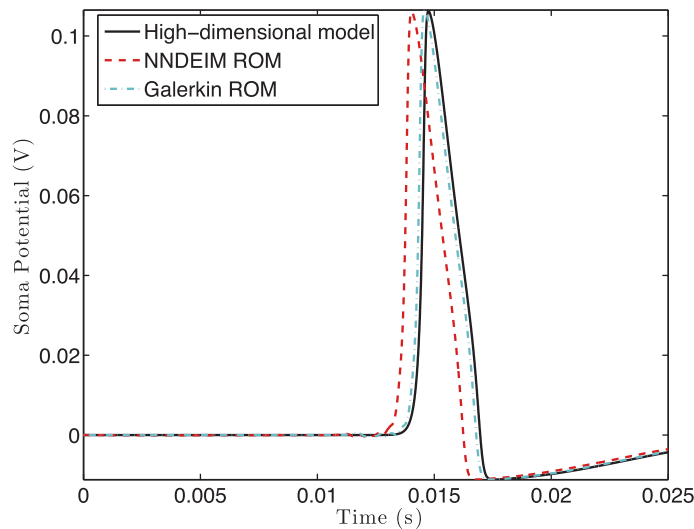
Fig. 10. *Comparison of the potential at the soma computed using the greedy NNDEIM approach with the high-dimensional response.*

ture preservation and the construction of nonnegative reduced bases. The capability of the proposed approach to generate accurate predictions in large-scale neuronal networks is demonstrated on the reduction of a system with more than 15,000 dofs.

Future work will focus on the development of hierarchical approaches similar to the one developed in [RB15] that can enable the simulation of potential propagation in networks of multiple neurons connected to each other.

Furthermore, parametric variations in cable geometry and physical properties will be considered using the parametric model reduction approaches developed in [AF08, ACCF09, AF11, PDTA15].

Appendix A. Expressions for the gating functions. The expressions for the coefficients α_m, α_h, α_n, β_m, β_h, and β_n are determined for the giant squid axon by Hodgkin and Huxley in [HH52] as

$$(A.1) \qquad \alpha_m(u) = \frac{10^5(0.025-u)}{e^{\frac{0.025-u}{0.01}} - 1}, \quad \beta_m(u) = 4 \times 10^3 e^{-\frac{u}{0.018}},$$

$$(A.2) \qquad \alpha_h(u) = 70 e^{-\frac{u}{0.02}}, \quad \beta_h(u) \frac{10^3}{e^{\frac{0.03-u}{0.01}} + 1},$$

$$(A.3) \qquad \alpha_n(u) = \frac{10^4(0.01-u)}{e^{\frac{0.01-u}{0.010}} - 1}, \quad \beta_n(u) = 125 e^{-\frac{u}{0.08}}.$$

Appendix B. Reduced equations for the model network. Starting from the components of (4.10) for cables 2 and 3, the time derivative term can be expanded as

$$\phi_k^{(c)^T} \mathbf{P}^{(c)} \mathbf{A}^{(c)} \mathbf{u}_{Rt}^{(c)} = \sum_{l=1}^{L^{(c)}} \phi_k^{(c)^T} \mathbf{P}^{(c)} \mathbf{A}^{(c)} \phi_l^{(c)} \frac{dq_l^{(c)}}{dt}(t) = \sum_{l=1}^{L^{(c)}} M_{kl}^{(c)} \frac{dq_l^{(c)}}{dt}(t),$$

the second term on the right-hand side as

$$-\frac{1}{C_m}\phi_k^{(c)T}\mathbf{P}^{(c)}\mathbf{A}^{(c)}\mathbf{G}_R^{(c)}(t)\mathbf{u}_R^{(c)} = -\frac{1}{C_m}\sum_{l=1}^{L^{(c)}}\phi_k^{(c)T}\mathbf{P}^{(c)}\mathbf{A}^{(c)}\mathbf{G}_R^{(c)}(t)\phi_l^{(c)}q_l^{(c)}(t)$$

$$= -\sum_{l=1}^{L^{(c)}}C_{kl}^{(c)}q_l^{(c)}(t),$$

and the first term in the right-hand side as

$$\mu\phi_k^{(c)T}\mathbf{Q}^{(c)}\left(\mathbf{A}^{(c)}\right)^2\mathbf{u}_{Rx}^{(c)}$$

$$= \mu\phi_k^{(c)T}\left(\mathbf{B}^{(c)} - \mathbf{Q}^{(c)T}\right)\left(\mathbf{A}^{(c)}\right)^2\mathbf{D}_1^{(c)}\mathbf{u}_R^{(c)}$$

$$= -\sum_{l=1}^{L^{(c)}}K_{kl}^{(c)}q_l(t) - \mu\left(a_0^{(c)}\right)^2\phi_{k0}^{(c)}u_{Rx0}^{(c)} + \mu\left(a_{N^{(c)}}^{(c)}\right)^2\phi_{kN^{(c)}}^{(c)}u_{RxN^{(c)}}^{(c)}.$$

The following series of small size matrices and vectors can then be defined for cables 2 and 3:
- $L^{(c)}$-by-$L^{(c)}$ constant symmetric matrices $\mathbf{M}_r^{(c)}$ with entries

$$M_{kl}^{(c)} = \phi_k^{(c)T}\mathbf{P}^{(c)}\mathbf{A}^{(c)}\phi_l^{(c)};$$

- $L^{(c)}$-by-$L^{(c)}$ time dependent diagonal matrices $\mathbf{C}_r^{(c)}(t)$ with entries

$$C_{kl}^{(c)} = \frac{1}{C_m}\phi_k^{(c)T}\mathbf{P}^{(c)}\mathbf{A}^{(c)}\mathbf{G}_R^{(c)}(t)\phi_l^{(c)};$$

- $L^{(c)}$-by-$L^{(c)}$ constant symmetric matrices $\mathbf{K}_r^{(c)}$ with entries

$$K_{kl}^{(c)} = \mu\phi_k^{(c)T}\left(\mathbf{D}_1^{(c)}\right)^T\mathbf{P}^{(c)}\left(\mathbf{A}^{(c)}\right)^2\mathbf{D}_1^{(c)}\phi_l^{(c)};$$

- small size vectors $\mathbf{d}_r^{(c)}(t)$ of size $L^{(c)}$ with entries

$$d_k^{(c)}(t) = \frac{1}{C_m}\phi_k^{(c)T}\mathbf{P}^{(c)}\mathbf{A}^{(c)}\mathbf{f}^{(c)}(t).$$

After adding the penalty terms associated with the BCs, the equation can then be written as

(B.1)
$$\sum_{l=1}^{L^{(c)}}M_{kl}^{(c)}\frac{dq_l^{(c)}}{dt}(t) = -\sum_{l=1}^{L^{(c)}}K_{kl}^{(c)}q_l^{(c)}(t) - \sum_{l=1}^{L^{(c)}}C_{kl}^{(c)}(t)q_l^{(c)}(t) + d_k^{(c)}(t)$$

$$+ \left(-\mu\left(a_{N^{(c)}}^{(c)}\right)^2 + \mu\left(a_{N^{(c)}}^{(c)}\right)^2\right)\phi_{kN^{(c)}}^{(c)}u_{RxN^{(c)}}^{(c)}$$

$$+ \left(\frac{\mu}{3} - \mu\right)\left(a_0^{(c)}\right)^2\phi_{k0}^{(c)}u_{Rx0}^{(c)} + \sum_{1\leq j\neq c\leq 3}\frac{\mu}{3}\left(a_0^{(c)}\right)^2\phi_{kx0}^{(c)}u_{R0}^{(c)}$$

$$+ \sum_{1\leq j\neq c\leq 3}\left(-\frac{\mu}{3}\left(a_0^{(c)}\right)^2\phi_{kx0}^{(c)}u_{R0}^{(j)} + \frac{\mu}{3}\phi_{k0}^{(c)}\left(a_0^{(j)}\right)^2 u_{Rx0}^{(j)}\right)$$

for $k = 1, \ldots, L^{(c)}, \ c = 1, \ldots, N_c$. After cancelation of terms (B.1) becomes

$$\sum_{l=1}^{L^{(c)}} M_{kl}^{(c)} \frac{dq_l^{(c)}}{dt}(t)$$

$$= -\sum_{l=1}^{L^{(c)}} \left(K_{kl}^{(c)} + \frac{2\mu}{3} \left(a_0^{(c)} \right)^2 \left(\phi_{k0}^{(c)} \phi_{lx0}^{(c)} - \phi_{kx0}^{(c)} \phi_{l0}^{(c)} \right) \right) q_l^{(c)}(t)$$

$$- \sum_{l=1}^{L^{(c)}} C_{kl}^{(c)}(t) q_l^{(c)}(t) + d_k^{(c)}(t)$$

$$+ \frac{\mu}{3} \sum_{1 \leq j \neq c \leq 3} \sum_{l=1}^{L^{(j)}} \left(- \left(a_0^{(c)} \right)^2 \phi_{kx0}^{(c)} \phi_{l0}^{(j)} + \left(a_0^{(j)} \right)^2 \phi_{k0}^{(c)} \phi_{lx0}^{(j)} \right) q_l^{(j)}(t), \quad k = 1, \ldots, L^{(c)},$$

leading to (4.11) when written in matrix form after the definition of matrices $\mathbf{K}_r^{(c_1, c_2)}$, $c_1 \neq c_2$. A similar derivation leads to the matrix form of the ODE associated with cable 1.

Appendix C. Energy estimate for the ROM of the model network.
Premultiplying (4.11) by $\mathbf{q}^{(c)}(t)$, omitting the source terms, and summing over $c = 1, \ldots, 3$, an energy estimate analog to the one derived in [AN13] can be constructed as follows:

$$(C.1) \qquad \sum_{c=1}^{3} \mathbf{q}^{(c)}(t)^T \mathbf{M}_r^{(c)} \frac{d\mathbf{q}^{(c)}}{dt}(t) = -\sum_{c=1}^{3} \mathbf{q}^{(c)}(t)^T (\mathbf{K}_r^{(c)} + \mathbf{C}_r^{(c)}(t)) \mathbf{q}^{(c)}(t)$$
$$+ \sum_{c=1}^{3} \sum_{1 \leq j \neq c \leq 3} \mathbf{q}^{(c)}(t)^T \mathbf{K}_r^{(c,j)} \mathbf{q}^{(j)}(t).$$

Since $K_{kl}^{(c,j)} = -K_{lk}^{(j,c)}$, the last term is

$$\sum_{c=1}^{3} \sum_{1 \leq j \neq c \leq 3} \mathbf{q}^{(c)}(t)^T \mathbf{K}_r^{(c,j)} \mathbf{q}^{(j)}(t)$$

$$= \sum_{c=1}^{3} \sum_{1 \leq j \neq c \leq 3} \sum_{k=1}^{L^{(c)}} \sum_{l=1}^{L^{(j)}} q_k^{(c)}(t) K_{kl}^{(c,j)} q_l^{(j)}(t)$$

$$= \sum_{1 \leq c < j \leq 3} \sum_{k=1}^{L^{(c)}} \sum_{l=1}^{L^{(j)}} \left(K_{kl}^{(c,j)} q_k^{(c)}(t) q_l^{(j)}(t) + K_{kl}^{(j,c)} q_k^{(j)}(t) q_l^{(c)}(t) \right)$$

$$= \sum_{1 \leq c < j \leq 3} \sum_{k=1}^{L^{(c)}} \sum_{l=1}^{L^{(j)}} \left(K_{kl}^{(c,j)} q_k^{(c)}(t) q_l^{(j)}(t) - K_{lk}^{(c,j)} q_k^{(j)}(t) q_l^{(c)}(t) \right)$$

$$= 0.$$

Similarly, it can be shown that summing over $c = 1, \ldots, 3$, the second terms in $\mathbf{K}_r^{(c)}$

cancel and (C.1) becomes

$$
\sum_{c=1}^{3} \mathbf{q}^{(c)}(t)^{T} \boldsymbol{\Phi}^{(c)T} \mathbf{P}^{(c)} \mathbf{A}^{(c)} \boldsymbol{\Phi}^{(c)} \frac{d\mathbf{q}^{(c)}}{dt}(t) + \frac{\mu}{\eta} \mathbf{q}^{(1)}(t)^{T} \boldsymbol{\Phi}^{(1)T} \mathbf{e}_{N^{(1)}+1}^{(1)} \mathbf{e}_{N^{(1)}+1}^{(1)}{}^{T} \boldsymbol{\Phi}^{(1)} \frac{d\mathbf{q}^{(1)}}{dt}
$$

$$
= -\sum_{c=1}^{3} \mathbf{q}^{(c)}(t)^{T} \left(\mu \boldsymbol{\Phi}^{(c)T} \mathbf{D}_{1}^{(c)T} \mathbf{P}^{(c)} \left(\mathbf{A}^{(c)} \right)^{2} \mathbf{D}_{1}^{(c)} \boldsymbol{\Phi}^{(c)} \right.
$$

$$
\left. - \frac{1}{C_m} \boldsymbol{\Phi}^{(c)T} \mathbf{P} \mathbf{A}^{(c)} \mathbf{G}_{R}^{(c)}(t) \boldsymbol{\Phi}^{(c)} \right) \mathbf{q}^{(c)}(t)
$$

$$
- \frac{\mu}{\eta C_m} \boldsymbol{\Phi}^{(1)T} \sqrt{\mathbf{G}_{R}^{(1)}(t)} \mathbf{e}_{N^{(1)}+1}^{(1)} \mathbf{e}_{N^{(1)}+1}^{(1)}{}^{T} \sqrt{\mathbf{G}_{R}^{(1)}(t)} \boldsymbol{\Phi}^{(1)} \mathbf{q}^{(1)}(t).
$$

Then,

$$
\frac{1}{2} \sum_{c=1}^{3} \left\| \sqrt{\mathbf{A}^{(c)}} \mathbf{u}_{R}^{(c)}(t) \right\|_{t}^{2} + \frac{\mu}{2\eta} \left(u_{RN^{(1)}}^{(1)}(t) \right)_{t}^{2}
$$

$$
= -\mu \sum_{c=1}^{3} \left\| \mathbf{A}^{(c)} \mathbf{u}_{Rx}^{(c)}(t) \right\|^{2} - \sum_{c=1}^{3} \left\| \sqrt{\frac{\mathbf{A}^{(c)} \mathbf{G}_{R}^{(c)}(t)}{C_m}} \mathbf{u}_{R}^{(c)}(t) \right\|^{2}
$$

$$
- \frac{\mu}{\eta} \left(\sqrt{\frac{g_{RN^{(1)}}^{(1)}(t)}{C_m}} u_{RN^{(1)}}^{(1)}(t) \right)^{2},
$$

leading to the energy estimate in terms of the weighted norm $\| \ \|_{\star}$.

Appendix D. Greedy algorithm for mask selection in NNDEIM. The greedy procedure for selecting the mask, initially developed for the GNAT method, is extended to the case of nonnegative bases and reported in Algorithm 2.

Appendix E. Proof of Proposition 5. Subtracting (3.10) from (7.3) leads, in terms of the error vector $\mathbf{e} = \mathbf{u}_R - \mathbf{u}$, to the following equality

$$
\mathbf{A}\mathbf{e}_t = \mu \mathbf{P}^{-1} \mathbf{Q} (\mathbf{A}^2 \mathbf{D}_1 \mathbf{e}) - \frac{1}{C_m} \mathbf{A} \left(\mathbf{G}_R(t)\mathbf{u}_R - \mathbf{G}(t)\mathbf{u} \right) + \frac{1}{C_m} \mathbf{A} \left(\mathbf{f}_R(t) - \mathbf{f}(t) \right)
$$

$$
+ \mathbf{p}_{\text{soma}}(\mathbf{e}) + \mathbf{p}_{\text{sealed}}(\mathbf{e}) + \mathbf{p}_{\text{junction}}(\mathbf{e}) + \mathbf{r}(t).
$$

Premultiplying by $\mathbf{e}^T \mathbf{P}$ gives

$$
\frac{1}{2} \frac{d}{dt} \left(\left\| \sqrt{\mathbf{A}} \mathbf{e} \right\|^{2} \right)
$$

$$
= \mu \mathbf{e}^T \mathbf{Q} \mathbf{A}^2 \mathbf{D}_1 \mathbf{e} + \frac{1}{C_m} \mathbf{e}^T \mathbf{P} \mathbf{A} \left(\mathbf{G}(t)\mathbf{u} - \mathbf{G}_R(t)\mathbf{u}_R \right) + \frac{1}{C_m} \mathbf{e}^T \mathbf{P} \mathbf{A} \left(\mathbf{f}_R(t) - \mathbf{f}(t) \right)
$$

$$
+ \mathbf{e}^T \mathbf{P} \left(\mathbf{p}_{\text{soma}}(\mathbf{e}) + \mathbf{p}_{\text{sealed}}(\mathbf{e}) + \mathbf{p}_{\text{junction}}(\mathbf{e}) \right) + \mathbf{e}^T \mathbf{P} \mathbf{r}(t).
$$

Algorithm 2 Greedy algorithm for mask selection

Require: ROBs $\widehat{\boldsymbol{\Psi}}_1$ and $\widehat{\boldsymbol{\Psi}}_2$ and basis dimension p
Ensure: Mask matrix $\mathbf{Z}$
1: $\mathbf{r}_1 = \psi_{11}$, $\mathbf{r}_2 = \psi_{21}$
2: $j = \operatorname{argmax}_m \left(\mathbf{r}_{1m}^2 + \mathbf{r}_{2m}^2 \right)$
3: $\mathbf{Z} = \mathbf{e}_j$
4: **for** $i = 2, \dots, p$ **do**
5:    Solve the nonnegative least-squares problems

$$\mathbf{c}_1 = \underset{\mathbf{z} \geq \mathbf{0}}{\operatorname{argmin}} \| \mathbf{Z}^T [\widehat{\psi}_{11}, \dots, \widehat{\psi}_{1(i-1)}] \mathbf{z} - \mathbf{Z}^T \psi_{1i} \|_2$$

   and

$$\mathbf{c}_2 = \underset{\mathbf{z} \geq \mathbf{0}}{\operatorname{argmin}} \| \mathbf{Z}^T [\widehat{\psi}_{21}, \dots, \widehat{\psi}_{2(i-1)}] \mathbf{z} - \mathbf{Z}^T \psi_{2i} \|_2$$

6:    Compute

$$\mathbf{r}_1 = \psi_{1i} - [\widehat{\psi}_{11}, \dots, \widehat{\psi}_{1(i-1)}] \mathbf{c}_1$$

   and

$$\mathbf{r}_2 = \psi_{2i} - [\widehat{\psi}_{21}, \dots, \widehat{\psi}_{2(i-1)}] \mathbf{c}_2$$

7:    $j = \operatorname{argmax}_m \left(\mathbf{r}_{1m}^2 + \mathbf{r}_{2m}^2 \right)$
8:    $\mathbf{Z} = [\mathbf{Z} \ \ \mathbf{e}_j]$
9: **end for**

The penalty terms are

$$\mathbf{e}^T \mathbf{P} \mathbf{p}_{\text{soma}}(\mathbf{e}) = -\frac{\mu}{\eta} \bigg(e_{tN^{(1)}}^{(1)} + \eta \left(a_{N^{(1)}}^{(1)} \right)^2 e_{xN^{(1)}}^{(1)}$$
$$+ \frac{1}{C_m} \left(\widehat{g}_{N^{(1)}}(t) u_{rN^{(1)}}^{(1)} - g_{N^{(1)}}(t) u_{N^{(1)}}^{(1)} \right) \bigg) e_{N^{(1)}}^{(1)},$$

$$\mathbf{e}^T \mathbf{P} \mathbf{p}_{\text{sealed}}(\mathbf{e}) = -\mu \sum_{c=1}^{3} \left(a_{N^{(c)}}^{(c)} \right)^2 \left(e_{xN^{(c)}}^{(c)} \right) e_{N^{(c)}}^{(c)},$$

$$\mathbf{e}^T \mathbf{P} \mathbf{p}_{\text{junction}}(\mathbf{e}) = \frac{\mu}{3} \sum_{c=1}^{3} \left(e_{x0}^{(c)} \sum_{j=1, j \neq c}^{3} \left(a_0^{(j)} \right)^2 \left(e_0^{(c)} - e_0^{(j)} \right) + e_0^{(c)} \sum_{j=1}^{3} \left(a_0^{(j)} \right)^2 e_{x0}^{(j)} \right).$$

Since $\mathbf{e}^T \mathbf{Q} \mathbf{A}^2 \mathbf{D}_1 \mathbf{e} = -\|\mathbf{A} \mathbf{D}_1 \mathbf{e}\|^2 + \sum_{j=1}^{3} ((a_{N^{(j)}}^{(j)})^2 e_{N^{(j)}}^{(j)} e_{xN^{(j)}}^{(j)} - (a_0^{(j)})^2 e_0^{(j)} e_{x0}^{(j)})$, the boundary summation cancels with most of the penalty terms, leading to the identity

$$\frac{1}{2} \frac{d}{dt} \left(\left\| \sqrt{\mathbf{A}} \mathbf{e} \right\|^2 \right) = -\mu \|\mathbf{A} \mathbf{D}_1 \mathbf{e}\|^2 + \frac{1}{C_m} \mathbf{e}^T \mathbf{P} \mathbf{A} \left(\mathbf{G}(t) \mathbf{u} - \mathbf{G}_R(t) \mathbf{u}_R \right) + \mathbf{e}^T \mathbf{P} \mathbf{r}(t)$$
$$+ \frac{1}{C_m} \mathbf{e}^T \mathbf{P} \mathbf{A} \left(\mathbf{f}_R(t) - \mathbf{f}(t) \right)$$
$$- \frac{\mu}{\eta} \left(e_{tN^{(1)}}^{(1)} + \frac{1}{C_m} \left(g_{RN^{(1)}}(t) u_{RN^{(1)}}^{(1)} - g_{N^{(1)}}(t) u_{N^{(1)}}^{(1)} \right) \right) e_{N^{(1)}}^{(1)}.$$

From

$$\mathbf{e}^T \mathbf{P} \mathbf{A} \left(\mathbf{G}(t) \mathbf{u} - \mathbf{G}_R(t) \mathbf{u}_R \right) = \mathbf{e}^T \mathbf{P} \mathbf{A} \left(\mathbf{G}(t) \left(\mathbf{u}_R - \mathbf{u} \right) + \left(\mathbf{G}(t) - \mathbf{G}_R(t) \right) \mathbf{u}_R \right)$$
$$= -\mathbf{e}^T \mathbf{P} \mathbf{A} \mathbf{G}(t) \mathbf{e} + \mathbf{e}^T \mathbf{P} \mathbf{A} \left(\mathbf{G}(t) - \mathbf{G}_R(t) \right) \mathbf{u}_R,$$

and similarly for the corresponding boundary term, one can write, in terms of the $\| \ \|_\star$ norm,

$$\frac{1}{2}\frac{d}{dt}\left(\|\mathbf{e}\|_\star^2\right)$$

$$= -\mu\|\mathbf{AD}_1\mathbf{e}\|^2 - \left\|\sqrt{\frac{\mathbf{G}(t)}{C_m}}\mathbf{e}\right\|_\star^2 + \mathbf{e}^T\mathbf{Pr}(t) + \frac{1}{C_m}\mathbf{e}^T\mathbf{PA}\left(\mathbf{f}_R(t) - \mathbf{f}(t)\right)$$

$$+ \frac{1}{C_m}\left(\mathbf{e}^T\mathbf{PA}\left(\mathbf{G}(t) - \mathbf{G}_R(t)\right)\mathbf{u}_R + \frac{\mu}{\eta}e_{N^{(1)}}^{(1)}\left(g_{N^{(1)}}(t) - g_{RN^{(1)}}(t)\right)u_{RN^{(1)}}^{(1)}\right).$$

Furthermore,

$$\mathbf{e}^T\mathbf{PA}\left(\mathbf{G}(t) - \mathbf{G}_R(t)\right)\mathbf{u}_R \leq \|\mathbf{e}\|\|\mathbf{A}(\mathbf{G}_R(t) - \mathbf{G}(t))\mathbf{u}_R\|$$
$$\leq C_1\|\mathbf{e}\|\|\mathbf{G}_R(t) - \mathbf{G}(t)\|_2\|\mathbf{u}_R\|_2$$

with $C_1 = \|\mathbf{A}\|$. Similarly,

$$\frac{\mu}{\eta}e_{N^{(1)}}^{(1)}\left(g_{N^{(1)}}(t) - g_{RN^{(1)}}(t)\right)u_{RN^{(1)}}^{(1)} \leq C_2\|\mathbf{e}\|\|\mathbf{G}_R(t) - \mathbf{G}(t)\|_2\|\mathbf{u}_R\|_2$$

with $C_2 = \frac{\mu}{\eta}\|\mathbf{A}\|$. Then, defining $C_G = \frac{C_1 + C_2}{C_m}$ and $C_f = \frac{C_1}{C_m}$,

$$\frac{1}{2}\frac{d}{dt}\left(\|\mathbf{e}\|_\star^2\right) + \mu\|\mathbf{AD}_1\mathbf{e}\|^2 + \left\|\sqrt{\frac{\mathbf{G}(t)}{C_m}}\mathbf{e}\right\|_\star^2 \leq \|\mathbf{e}\|B(t)$$

and, since $\|\mathbf{e}\| \leq \frac{1}{\min_i \sqrt{a_i}}\|\mathbf{e}\|_*$,

$$\frac{1}{2}\frac{d}{dt}\left(\|\mathbf{e}\|_\star^2\right) + \left\|\sqrt{\frac{\mathbf{G}(t)}{C_m}}\mathbf{e}\right\|_\star^2 \leq \frac{1}{\min_i \sqrt{a_i}}\|\mathbf{e}\|_\star B(t).$$

Since $g_i(t) \geq g_{\min} > 0$,

$$\left\|\sqrt{\frac{\mathbf{G}(t)}{C_m}}\mathbf{e}\right\|_\star^2 \geq \frac{g_{\min}}{C_m}\|\mathbf{e}\|_\star^2$$

and, dividing by $\|\mathbf{e}(t)\|_\star$,

$$\frac{d}{dt}\|\mathbf{e}(t)\|_\star + \frac{g_{\min}}{C_m}\|\mathbf{e}(t)\|_\star \leq \frac{1}{\min_i \sqrt{a_i}}B(t).$$

Letting $\delta_0 = \frac{g_{\min}}{C_m}$, this leads to inequality (7.1) after time integration.

Appendix F. Proof of Proposition 6.   Starting from

$$\|\widehat{\mathbf{G}}_R(t) - \mathbf{G}(t)\|_2 \leq \|\widehat{\mathbf{G}}_R(t) - g_3\mathbf{I}\|_2 + \|\mathbf{G}(t) - g_3\mathbf{I}\|_2 \leq \left\|\widehat{\mathbf{G}}_R(t) - g_3\mathbf{I}\right\|_2 + \sum_{j=1}^{2}g_j,$$

one can bound the first term as

$$\|\widehat{\mathbf{G}}_R(t) - g_3\mathbf{I}\|_2 \leq \sum_{j=1}^{2} g_j\|\widehat{\boldsymbol{\Psi}}_j\mathbf{p}_j(t)\|_\infty \leq \sum_{j=1}^{2} g_j\|\widehat{\boldsymbol{\Psi}}_j\|_2\|\mathbf{p}_j(t)\|_2.$$

Furthermore, with the property $\mathbf{m}(t) \leq 1$, $\mathbf{h}(t) \leq 1$, and $\mathbf{n}(t) \leq 1$ shown in [AN13],

$$\|\mathbf{Z}^T\widehat{\boldsymbol{\Psi}}_1\mathbf{p}_1\|_2 - \|\mathbf{Z}^T(\mathbf{m}^3 \odot \mathbf{h})\|_2 \leq \|\mathbf{Z}^T(\mathbf{m}^3 \odot \mathbf{h}) - \mathbf{Z}^T\widehat{\boldsymbol{\Psi}}_1\mathbf{p}_1\|_2$$
$$\leq \|\mathbf{Z}^T(\mathbf{m}^3 \odot \mathbf{h})\|_2 \leq n_c\|\mathbf{Z}^T(\mathbf{m}^3 \odot \mathbf{h})\|_\infty \leq n_c.$$

Since $\|\mathbf{Z}^T\widehat{\boldsymbol{\Psi}}_1\mathbf{p}_1\|_2 - \|\mathbf{Z}^T(\mathbf{m}^3 \odot \mathbf{h})\|_2 \leq \|\mathbf{Z}^T(\mathbf{m}^3 \odot \mathbf{h}) - \mathbf{Z}^T\widehat{\boldsymbol{\Psi}}_1\mathbf{p}_1\|_2$, this leads to $\|\mathbf{Z}^T\widehat{\boldsymbol{\Psi}}_1\mathbf{p}_1\|_2 \leq 2n_c$ and

$$\|\mathbf{p}_1\|_2 \leq \frac{2n_c}{\sigma_{\min}(\mathbf{Z}^T\widehat{\boldsymbol{\Psi}}_j)}.$$

A similar inequality holds for $\mathbf{p}_2$ and hence

$$\|\mathbf{G}_R(t) - g_3\mathbf{I}\|_2 \leq \sum_{j=1}^{2} g_j \left(1 + \frac{2n_c\|\widehat{\boldsymbol{\Psi}}_j\|_2}{\sigma_{\min}(\mathbf{Z}^T\widehat{\boldsymbol{\Psi}}_j)}\right).$$

Similarly, $\|\widehat{\mathbf{f}}_R(t) - \mathbf{f}(t)\|_2$ can be bounded as

$$\|\widehat{\mathbf{f}}_R(t) - \mathbf{f}(t)\|_2 \leq \sum_{j=1}^{2} g_j \, |E_j| \left(1 + \frac{2n_c\|\widehat{\boldsymbol{\Psi}}_j\|_2}{\sigma_{\min}(\mathbf{Z}^T\widehat{\boldsymbol{\Psi}}_j)}\right),$$

leading to the result.

REFERENCES

[ACCF09] D. AMSALLEM, J. CORTIAL, K. CARLBERG, AND C. FARHAT, *A method for interpolating on manifolds structural dynamics reduced-order models*, Internat. J. Numer. Methods Engrg., 80 (2009), pp. 1241–1258.

[AF08] D. AMSALLEM AND C. FARHAT, *Interpolation method for adapting reduced-order models and application to aeroelasticity*, AIAA Journal, 46 (2008), pp. 1803–1813.

[AF11] D. AMSALLEM AND C. FARHAT, *An online method for interpolating linear parametric reduced-order models*, SIAM J. Sci. Comput., 33 (2011), pp. 2169–2198.

[AF12] D. AMSALLEM AND C. FARHAT, *Stabilization of projection-based reduced-order models*, Internat. J. Numer. Methods Engrg., 91 (2012), pp. 358–377.

[AF13] D. AMSALLEM AND C. FARHAT, *On the stability of reduced-order linearized computational fluid dynamics models based on POD and Galerkin projection: Descriptor vs non-descriptor forms*, MS&A. Model. Simul. Appl., (2013).

[AFZ13] D. AMSALLEM, C. FARHAT, AND M. J. ZAHR, *On the robustness of residual minimization for constructing POD-based reduced-order CFD models*, 21st AIAA Computational Fluid Dynamics Conference, San Diego, CA, 2013, Curran, Red Hook, NY, 2013, pp. 1–18.

[AH15] D. AMSALLEM AND U. HETMANIUK, *A posteriori error estimators for linear reduced-order models using Krylov-based integrators*, Internat. J. Numer. Methods Engrg., 102 (2015), pp. 1238–1261.

[AN13] D. AMSALLEM AND J. NORDSTRÖM, *High-order accurate difference schemes for the Hodgkin–Huxley equations*, J. Comput. Phys., 252 (2013), pp. 573–590.

[AR11] D. AMSALLEM AND J. ROYCHOWDHURY, *ModSpec: An open, flexible specification framework for multi-domain device modelling*, IEEE/ACM Conference on Computer-Aided Design, IEEE, Piscataway, NJ, 2011, pp. 367–374.

[AZF12]   D. Amsallem, M. J. Zahr, and C. Farhat, *Nonlinear model order reduction based on local reduced-order bases*, Internat. J. Numer. Methods Engrg., 92 (2012), pp. 891–916.

[BD09]   B. N. Bond and L. Daniel, *Stable reduced models for nonlinear descriptor systems through piecewise-linear approximation and projection*, IEEE Trans. Comput.-Aided Des. Integrated Circuits Syst., 28 (2009), pp. 1467–1480.

[BGM⁺14]   B. V. Benjamin, P. Gao, E. McQuinn, S. Choudhary, A. R. Chandrasekaran, J. M. Bussat, R. Alvarez-Icaza, J. V. Arthur, P. A. Merolla, and K. Boahen, *Neurogrid: A mixed-analog-digital multichip system for large-scale neural simulations*, in Proc. IEEE, 102 (2014), pp. 699–716.

[BKST09]   M. F. Barone, I. Kalashnikova, D. J. Segalman, and H. K. Thornquist, *Stable Galerkin reduced order models for linearized compressible flow*, J. Comput. Phys., 228 (2009), pp. 1932–1946.

[BMNP04]   M. Barrault, Y. Maday, N. C. Nguyen, and A. T. Patera, *An empirical interpolation method: Application to efficient reduced-basis discretization of partial differential equations*, C. R. Acad. Sci. Paris Ser. I, 339 (2004), pp. 667–672.

[CBMF11]   K. Carlberg, C. Bou-Mosleh, and C. Farhat, *Efficient non-linear model reduction via a least-squares Petrov–Galerkin projection and compressive tensor approximations*, Internat. J. Numer. Methods Engrg., 86 (2011), pp. 155–181.

[CFCA13]   K. Carlberg, C. Farhat, J. Cortial, and D. Amsallem, *The GNAT method for nonlinear model reduction: Effective implementation and application to computational fluid dynamics and turbulent flows*, J. Comput. Phys., 242 (2013), pp. 623–647.

[CGA94]   M. H. Carpenter, D. Gottlieb, and S. Abarbanel, *Time-stable boundary conditions for finite-difference schemes solving hyperbolic systems: Methodology and application to high-order compact schemes*, J. Comput. Phys., 111 (1994), pp. 220–236.

[CS10]   S. Chaturantabut and D. C. Sorensen, *Nonlinear model reduction via discrete empirical interpolation*, SIAM J. Sci. Comput., 32 (2010), pp. 2737–2764.

[DPW14]   W. Dahmen, C. Plesken, and G. Welper, *Double greedy algorithms: Reduced basis methods for transport dominated problems*, ESAIM Math. Model. Numer. Anal., 48 (2014), pp. 623–663.

[GKO95]   B. Gustafsson, H.-O. Kreiss, and J. Oliger, *Time Dependent Problems and Difference Methods*, Wiley-Interscience, New York, 1995.

[HH52]   A. Hodgkin and A. F. Huxley, *A quantitative description of membrane current and its application to conduction and excitation in nerve*, J. Physiol., 117 (1952), pp. 500–544.

[Hin84]   M. Hines, *Efficient computation of branched nerve equations*, Internat. J. Bio-Med. Comput., 15 (1984), pp. 69–76.

[KCSC10]   A. R. Kellems, S. Chaturantabut, D. C. Sorensen, and S. J. Cox, *Morphologically accurate reduced order modeling of spiking neurons*, J. Comput. Neurosci., 28 (2010), pp. 477–494.

[KHP13]   J. Kim, Y. He, and H. Park, *Algorithms for nonnegative matrix and tensor factorizations: A unified view based on block coordinate descent framework*, J. Global Optim., 58 (2013), pp. 285–319.

[KP08]   J. Kim and H. Park, *Toward faster nonnegative matrix factorization: A new algorithm and comparisons*, in 2008 Eighth IEEE International Conference on Data Mining (ICDM), IEEE Computer Society, Los Alamitos, CA, 2008, pp. 353–362.

[KS74]   H.-O. Kreiss and G. Scherer, *Finite element and finite difference methods for hyperbolic partial differential equations*, in Mathematical Aspects of Finite Elements in Partial Differential Equations, Academic, New York, 1974, pp. 195–212.

[KS75]   H.-O. Kreiss and G. Scherer, *On the existence of energy estimates for difference approximations for hyperbolic systems*, Technical report, Department of Scientific Computing, Uppsala University, Uppsala, Sweden, 1975.

[KS09]   J. P. Keener and J. Sneyd, *Mathematical Physiology*, 2nd ed., Springer Verlag, New York, 2009.

[LS99]   D. D. Lee and H. S. Seung, *Learning the parts of objects by non-negative matrix factorization*, Nature, 401 (1999), pp. 788–791.

[Mat12]   K. Mattsson, *Summation by parts operators for finite difference approximations of second-derivatives with variable coefficients*, J. Sci. Comput., 51 (2012), pp. 650–682.

[NFA03]   J. NORDSTRÖM, K. FORSBERG, AND C. ADAMSSON, *Finite volume methods, unstructured meshes and strict stability for hyperbolic problems*, Appl. Numer. Math., 45 (2003), pp. 453–473.

[NL13]   J. NORDSTRÖM AND T. LUNDQVIST, *Summation-by-parts in time*, J. Comput. Phys., (2013).

[NS05]   J. NORDSTRÖM AND M. SVÄRD, *Well-posed boundary conditions for the Navier–Stokes equations*, SIAM J. Numer. Anal., 43 (2005), pp. 1231–1255.

[Ols95a]   P. OLSSON, *Summation by parts, projections, and stability.* I, Math. Comp., 64 (1995), pp. 1035–1065.

[Ols95b]   P. OLSSON, *Summation by parts, projections, and stability.* II, Math. Comp., 64 (1995), pp. 1473–1493.

[PDTA15]   A. PAUL-DUBOIS-TAINE AND D. AMSALLEM, *An adaptive and efficient greedy procedure for the optimal training of parametric reduced-order models*, Internat. J. Numer. Methods Engrg., 102 (2015), pp. 1262–1292.

[RB15]   J. ROYCHOWDHURY AND P. BHUSHAN, *Hierarchical abstraction of weakly coupled synchronized oscillator networks*, Internat. J. Numer. Methods Engrg., 102 (2015), pp. 1041–1076.

[RV07]   G. ROZZA AND K. VEROY, *On the stability of the reduced basis method for Stokes equations in parametrized domains*, Comput. Methods Appl. Mech. Engrg., 196 (2007), pp. 1244–1260.

[Sir87]   L. SIROVICH, *Turbulence and the dynamics of coherent structures. Part* I: *Coherent structures*, Quart. Appl. Math., 45 (1987), pp. 561–571.

[Str94]   B. STRAND, *Summation by parts for finite difference approximations for d/dx*, J. Comput. Phys., 110 (1994), pp. 47–67.

[UP14]   K. URBAN AND A. T. PATERA, *An improved error bound for reduced basis approximation of linear parabolic problems*, Math. Comp., 83 (2014), pp. 1599–1615.